DEPARTMENT OF CHEMISTRY, UNIVERSITY OF JYVÄSKYLÄ
RESEARCH REPORT No. 188

# PHOTODYNAMICS STUDIES OF LIGAND-PROTECTED GOLD NANOCLUSTERS BY USING ULTRAFAST TRANSIENT INFRARED SPECTROSCOPY

BY

**SATU MUSTALAHTI**

Academic Dissertation for the Degree of
Doctor of Philosophy

*To be presented, by permission of the Faculty of Mathematics and Science of the University of Jyväskylä, for public examination in KEM4, on December 11th, 2015 at 12 noon.*

UNIVERSITY OF JYVÄSKYLÄ


Jyväskylä, Finland
ISBN 978-951-39-6418-4
ISSN 0357-346X

# ABSTRACT

Mustalahti, Satu
Photodynamics studies of ligand-protected gold nanoclusters by using ultrafast transient infrared spectroscopy
Jyväskylä: University of Jyväskylä, 2015, 58 p.
(Department of Chemistry, University of Jyväskylä Research Report Series
ISSN 0357-346X)
ISBN 978-951-39-6418-4

Highly monodisperse samples of three ligand-protected gold nanoclusters $Au_{102}(p\text{MBA})_{44}$, $Au_{144}(SC_2H_4Ph)_{60}$, and a cluster tentatively identified as $Au_{130}(p\text{MBA})_{50}$, were characterized by UV/vis and infrared spectroscopy, and their photodynamics was studied by transient absorption spectroscopy. The dynamics study for each cluster was performed by electronically exciting the cluster with a pump pulse in the visible or near infrared region and by monitoring the transient absorption of vibrational modes of the ligands with a mid-IR probe pulse. The photodynamics studies were used to determine the molecular or metallic behavior of the cluster, and also to gain important size dependent information about the relaxation processes and energy states involved in them.

A drastic difference between the relaxation dynamics is observed between $Au_{102}(p\text{MBA})_{44}$ and $Au_{130}(p\text{MBA})_{50}$ clusters when compared to $Au_{144}(SC_2H_4Ph)_{60}$, which clearly shows that the two smaller clusters show molecular behavior, while the $Au_{144}$ species shows relaxation typical for metallic species. Based on this, the transition region between molecular and metallic behavior for gold can be narrowed to occur between 130 and 144 gold atoms.

By combining the experimental results with energies of the electronic states of the clusters obtained from DFT calculations, the observed photodynamics for the molecular clusters could be explained. For both clusters, the relaxation was shown to involve relaxation via triplet states, and also revealed a vital role of the relative energies of different energy states in singlet and triplet manifolds. Vibrational cooling was also found to have a significant role in the relaxation, since the excess vibrational energy in the hot system was found to facilitate the observed relaxation processes.

Keywords: gold nanocluster, femtosecond, ultrafast spectroscopy, electronic relaxation, transient absorption, $Au_{102}(p\text{MBA})_{44}$, $Au_{144}(SR)_{60}$, $Au_{130}$, vibrational spectroscopy

**Author's address**

Satu Mustalahti
Department of Chemistry
Nanoscience Center
University of Jyväskylä
P.O. Box 35
FI-40014 University of Jyväskylä
satu.a.mustalahti@jyu.fi

**Supervisors**

Professor Mika Pettersson
Department of Chemistry
Nanoscience Center
University of Jyväskylä
P.O. Box 35
FI-40014 University of Jyväskylä

**Reviewers**

Professor Nikolai Tkatchenko
Department of Chemistry and Bioengineering
Tampere University of Technology
Finland

Dr. Jan Helbing
Department of Chemistry
University of Zürich
Switzerland

**Opponent**

Associate Professor Kenneth L. Knappenberger, Jr.
Department of Chemistry and Biochemistry
Florida State University
USA

# PREFACE

The work presented in this thesis has been carried out at the Department of Chemistry, Nanoscience Center, University of Jyväskylä in 2012–2015, and was funded by The National Doctoral Programme in Nanoscience (NGS-NANO), which is gratefully acknowledged.

I am deeply grateful for my supervisor Prof. Mika Pettersson for introducing me to this very interesting thesis project. I would also like to thank him for all his guidance and for believing in me throughout the project. In addition, I am extremely grateful for Pasi Myllyperkiö for his guidance and priceless help throughout the project, and for teaching me everything I know about practical laser spectroscopy. I am also grateful for the reviewers of this thesis for their valuable comments that really helped to improve this thesis.

None of the work presented here could have been done without a very inspiring collaboration that I have been privileged to be a small part of. I would like to thank Prof. Hannu Häkkinen for helping me to understand the fascinating world of nanoclusters. In particular, I would also like to thank Tanja Lahtinen for providing me with the samples, even if I asked for ridiculously large amounts of them, and Sami Malola for all nice figures and also for the computational results that proved out to be essential for all of my work. Kirsi Salorinne, Tiia-Riikka Tero and Jaakko Koivisto are also gratefully acknowledged for analyzing the samples and for their support. I am also grateful for Gerrit Groenhof for broadening my scientific knowledge by introducing me to my almost two-day side project.

In addition, I am very grateful for several past and present colleagues. I would especially like to thank Heli Lehtivuori and Liisa Antila for their guidance, support, and friendship during my thesis work. I would also like to thank Heikki Häkkänen for many interesting discussions and useful tips regarding the experiments and Jukka Aumanen for his company on various conference trips. A special thank you is also owed to my office roommates Anna Kausamo and Mikko Väärämäki for their support, several interesting discussions, and for tolerating my company on a daily basis. Finally, I would also like to thank everyone else at nanoscience center and chemistry department for all your contributions in creating an interesting and supporting working environment.

For everything else needed to complete this thesis I am indebted beyond words to my family and relatives. I would like to express my heartfelt gratitude especially to my parents Tarja and Hannu, and my beloved siblings Kati, Pauli and Anni for their endless support, encouragement, and understanding.

Jyväskylä, November 2015

*Satu Mustalahti*

## LIST OF ORIGINAL PUBLICATIONS

This thesis is based on original publications listed below. In the following text, they are referred to by their Roman numerals.

I Satu Mustalahti, Pasi Myllyperkiö, Tanja Lahtinen, Kirsi Salorinne, Sami Malola, Jaakko Koivisto, Hannu Häkkinen and Mika Pettersson, Ultrafast Electronic Relaxation and Vibrational Cooling Dynamics of $Au_{144}(SC_2H_4Ph)_{60}$ Nanocluster Probed by Transient Mid-IR Spectroscopy, *J. Phys. Chem. C*, **2014**, *118*, 18233–18239.

II Satu Mustalahti, Pasi Myllyperkiö, Sami Malola, Tanja Lahtinen, Kirsi Salorinne, Jaakko Koivisto, Hannu Häkkinen and Mika Pettersson, Molecule-like Photodynamics of $Au_{102}(p\text{MBA})_{44}$ Nanocluster, *ACS Nano*, **2015**, *9*, 2328–2335.

III Satu Mustalahti, Pasi Myllyperkiö, Tanja Lahtinen, Sami Malola, Kirsi Salorinne, Tiia-Riikka Tero, Jaakko Koivisto, Hannu Häkkinen and Mika Pettersson, Photodynamics of a Molecular Water-Soluble Nanocluster Identified as $Au_{130}(p\text{MBA})_{50}$, *J. Phys. Chem. C*, **2015**, *119*, 20224–20229.

The author is the primary author of papers I–III. She has performed most of the spectroscopic experiments and data-analysis in all papers and participated in writing papers I and II. She wrote the first draft of paper III.

## ABBREVIATIONS

| | |
|---|---|
| *p*MBA | para-mercaptobenzoic acid |
| UV | ultraviolet |
| vis | visible |
| IR | infrared |
| DFT | density functional theory |
| CD | circular dichroism |
| HOMO | highest occupied molecular orbital |
| LUMO | lowest unoccupied molecular orbital |
| LDM | liquid drop model |
| LSPR | localized surface plasmon resonance |
| NMR | nuclear magnetic resonance |
| FTIR | Fourier transform infrared |
| MCT detector | mercury cadmium tellurium (HgCdTe) detector |
| BS | beam splitter |
| GS | ground state |
| VR | vibrational relaxation |
| IC | internal conversion |
| ISC | intersystem crossing |
| FL | fluorescence |
| PH | phosphorescence |
| SDS- | sodium dodecyl sulfate |
| PAGE | polyacrylamide gel electrophoresis |
| DCM | dichloromethane |
| OPA | optical parametric amplifier |
| NIR | near infrared |
| PET | phenylethanethiol ($HSC_2H_4Ph$) |

# CONTENTS

# 1 INTRODUCTION

The utilization of gold in human history spans from ancient civilizations to present day society.[1] Due to its many unique properties and high value, gold has always been one of the most sought after elements. It has been widely used, for example, as currency and jewelry and has also been given significant symbolic value. Although already studied and utilized for millennia, gold has found a central role and renewed research interest in modern nanoscience research in the form of nanoclusters and particles.

Nanoscience is a relatively new research field that focuses on a variety of sample systems that fall in the size range of about 1–100 billionths of a meter, namely 1–100 nanometers. Nanoscience is by nature a highly interdisciplinary field combining knowledge from chemistry, physics, and biology in an effort to study various nanoscale systems from supramolecular assemblies, carbon nanotubes, and nanoclusters to biological entities, such as proteins and viruses. One of the popular research topics in this field is nano-sized clusters that lie on the borderline between chemistry, physics and material science.[2] The clusters represent a form of matter different from both the bulk form and the atomic systems. This type of clusters can be formed from atoms or molecules and from a variety of elements, including gold.

Nano-sized objects can be studied by several methods to obtain versatile information about their structure and properties. One of the methods commonly used is optical spectroscopy, in which the interaction between light and matter is utilized to determine properties of the sample that are related to energy states. [3–5] Spectroscopy can also be extended to obtain time dependent information by utilizing short excitation pulses. In many cases, time-resolved information in the time scale relevant to nuclear motions is required. For these studies, ultrafast spectroscopy on the femtosecond time scale is needed. This type of research falls into the field of femtochemistry[6], which is a modern research field dedicated to processes occurring in billionths of a microsecond.

In the work presented in this thesis,[I-III] ultrafast femtosecond spectroscopy in mid-IR region is used to study in detail the photophysics of ligand-protected gold nanoclusters in three different sizes. The studied clusters are of particular

interest since they fall into a size range close to the transition between molecular and metallic cluster behavior. The study presented here involves experiments, in which the relaxation dynamics of the electronic excitation of the clusters is monitored by studying the changes in the vibrational modes of the ligand molecules. These results can be used to obtain fundamental size-dependent information on the clusters and to narrow the transition region between molecular and metallic behavior.

# 2 BACKGROUND

## 2.1 General chemical and physical properties of gold

The atomic number of gold (Au) is 79, and it is a member of group 11 in the periodic table of elements together with copper and silver. In the electronic ground state, a gold atom has a filled 5d electronic shell and the electronic configuration [Xe]$4f^{14}5d^{10}6s^{1}$. [1,7,8] In chemical compounds, the oxidation state of gold is usually either Au(III) or Au(I), of which Au(III) is dominant. Rarer oxidation states observed for gold include Au(V), which is found only in $AuF_5$ and $AuF_6^-$, and Au(II). In some compounds, gold can also be found in the anionic form as the auric anion Au(-I). Metallic gold has an fcc (face-centered cubic) crystal lattice. In the metallic form, gold has a characteristic yellow color and is a highly malleable non-magnetic and non-toxic metal that can be alloyed with other metals. Chemically, gold is very inert, allowing it to be observed in pure metallic form in nature.

Gold has many unique properties among metals and even among the group 11 metals. Many of these properties can be explained by electronic structure and relativistic effects that play a significant role for gold.[1,7,8] The electronic structure of metallic gold is inherited from the electronic structure of individual gold atoms as the increasing number of atoms causes the electronic levels to form a band structure. Electrons of the filled gold d orbitals form a d-band filled with electrons. The conduction band of gold is then formed from 6s and 6p orbitals. The interband transition threshold between the d-band and the conduction band is 1.84 eV, which corresponds to red part of the visible spectrum. The interband transition is also responsible for the characteristic color of metallic gold. The chemical bonding in metallic systems is generally described by free valence electrons moving in the potential provided by the nuclei.

## 2.2 Gold nanoclusters and motivation for their studies

Clusters are a unique form of material on the borderline between the atomic level and bulk material.[2] In principle, clusters can be obtained by cutting metallic gold into smaller pieces or by growing them by combining individual atoms. The exact definition of a cluster varies slightly depending on the source, but in general, cluster research concerns the study of particles with size varying from few atoms to up to thousands of atoms.[2,9] Particles of this size fall into the nanoscale region for which they can be referred to as nanoclusters. Clusters can be divided into different size ranges depending on the number of atoms and hence the size of the cluster. The division is often made so that the small clusters with properties closer to those of molecules and individual atoms are separated from the larger nanoparticles and nanocrystals.[10] Although this thesis concerns only gold species, it should be noted that clusters can also be made from other metals, molecules, or even noble gases.[2]

At the moment, clusters have gathered an enormous amount of interest in the scientific community, and the field is developing and expanding rapidly. Both fundamental and applied research is currently performed. Gold clusters can be obtained by using several methods, and they can be studied in gas phase, in solution, and by supporting them on surfaces.[1,2,10] By using modern research methods, many different cluster properties can now be addressed, which has significantly contributed to the development of the field.

Much of the interest directed towards gold clusters is related to their properties and their utilization in various applications.[1,11,12] Due to their size and structure, gold clusters have unique properties that differ greatly from both the properties of small chemical gold compounds and the metallic gold presented in the previous chapter. These properties include, for example, the size dependent optical, electronic, and photothermal properties, and catalytic activity, which is significantly increased when compared to that of metallic gold.[1,2] These features are highly attractive towards many applications, for example, in photonics, sensors, medicine, and biochemistry. [1,11,12]

From the point of view of fundamental research, clusters provide an ideal class of compounds to study the evolvement of the bulk properties from the properties of individual atoms.[2] Especially for metals, this provides a possibility to study the evolvement of the atomic geometry to the fcc lattice and the emergence of common metallic properties, such as the electric conductivity.[2] One of the important fundamental aspects that can also be addressed is determining the number of metal atoms that is needed to make the system metallic. This type of possibility to correlate the size of the cluster with its properties also serves as motivation for the research presented in this thesis.

## 2.3 Thiol protected gold nanoclusters

One of the problems related to gold nanoclusters is that some sort of protection is generally needed in order to prevent aggregation into larger particles at high concentrations.[10] Therefore, in recent years, particular interest has been directed towards monolayer protected particles and especially thiolate protected nanoclusters.[10,13] In these systems, a layer of covalently bonded ligands is attached to the cluster surface to protect the metallic core. The protecting ligand layer prevents cluster aggregation making them stable in ambient conditions. Compared to unprotected gas phase clusters, the protected ones are attractive for many reasons. The additional stability allows the clusters to be handled like chemicals, which facilitates studies and applications inaccessible to gas phase clusters. In addition, the ligand layer has a significant effect on the cluster properties and can also be modified.

The interaction between gold and sulfur plays a key role in the thiol protected clusters.[14] The strength of covalent Au–S interaction is close to the Au–Au bond. Therefore, the bonding in the gold surface is modified by the interaction with sulfur. In addition to protected clusters, the bonding between gold and sulfur has been studied in self-assembled monolayers on gold surfaces and in molecular junctions in gold electrodes in molecular electronics applications.[14,15] In addition to sulfur, phosphorus also has high affinity towards gold. Hence, phosphines can also be used as ligands for gold clusters.[10]

### 2.3.1 Synthesis

Colloidal solutions of gold have been known for hundreds of years.[1] However, the synthesis of nanometer-sized thiol protected clusters was first introduced in 1994 by Brust et al.[16] The introduction of a synthesis method has facilitated a large experimental effort focusing on these systems, and different modifications of the synthesis are used to obtain clusters with different sizes and different ligands.[17–19] For example, thiols with different alkyl chains and thiols containing carboxylic acid groups are generally used as ligands.[17–19] In addition, more complex molecules, such as glutathione, and protein units with thiol group containing cysteine residues have been used.[20–22]

In general, the cluster synthesis includes two major steps.[16] Gold is added to the reaction mixture as Au(III) ions by using $AuCl_4^-$ salt. The gold ions are first reduced by thiols to form a Au–S–Au–S polymer. The polymer is then further reduced to form the clusters by adding sodium borohydride ($NaBH_4$) to the mixture. The exact reaction mechanism of the cluster formation and the ligand induced effects on this process are not fully known. Variations to the synthesis can be introduced, for example, by changing the molar ratio between gold and thiols.[19] Other methods to produce thiol protected clusters include a synthesis of phosphine protected clusters followed by a ligand exchange with thiols, and

a method in which polymer stabilized clusters are first prepared and then thiolated by adding the thiol ligand.[10]

The synthesis procedures generally produce a polydisperse cluster size distribution. To separate different cluster sizes, partial precipitation procedures or liquid chromatography can be used.[17,19,23] Much of the recent research effort in synthesis has been dedicated to optimizing the synthesis to produce monodisperse cluster samples with different cluster sizes and different ligands.[17,18,24] Some highly stable cluster sizes can also be made by first making polydisperse samples of larger clusters and then using excess amount of thiol to etch the cluster to form the most stable species. This kind of procedure is called the size-focusing method.[23]

### 2.3.2 General structure of thiol-protected gold nanoclusters

Due to their structure, thiol-protected gold clusters provide a quite unique sample system, because they combine metallic gold to small organic ligand molecules. As stated, the thiol-protected clusters consist of a metallic gold core protected by covalently bonded thiolate ligands. The exact structure of all thiol protected clusters was not known until the crystal structure of $Au_{102}(p\text{MBA})_{44}$ (*p*MBA=*para*-mercaptobenzoic acid) was solved in 2007 by x-ray crystallography.[25] Following the first structure determination, the structures of several clusters having different size and different ligands have been determined. These species include, for example, $Au_{25}$, $Au_{38}$, $Au_{68}$, $Au_{130}$, and $Au_{133}$.[26–30] The exact structure determination can be done by x-ray crystallography or by high resolution electron microscopy.[25,30] To deduce an exact cluster composition in the form of core size and the number of ligand molecules, mass spectrometry with help of elemental analysis can also be used.[19,31] Because the exact structure of many of the small thiol-protected clusters is known, special interest has been directed towards studying them.

The general structure of the clusters can be understood to consist of three parts: an inner gold core, which is covered by a surface layer that includes the gold atoms bonded to the ligands, and finally the outer ligand layer.[25,32] The inner core is generally metallic, and the gold atoms have a formal charge of 0. The surface layer consists of gold-sulfur motifs, where the gold has a formal +1 charge, while the sulfur atoms have a formal -1 charge. The surface layer consists of protecting gold–sulfur motifs that can have different structures. These structures commonly include shorter S–Au–S units and longer S–Au–S–Au–S units.[25-29] This type of structure where the gold core of the cluster is divided into metallic part and the protecting motifs, is referred to as the divide and protect model.[32] The outer ligand layer consists of the organic parts of the ligands. As an example, the structure of $Au_{102}(p\text{MBA})_{44}$ is shown in Fig. 1.

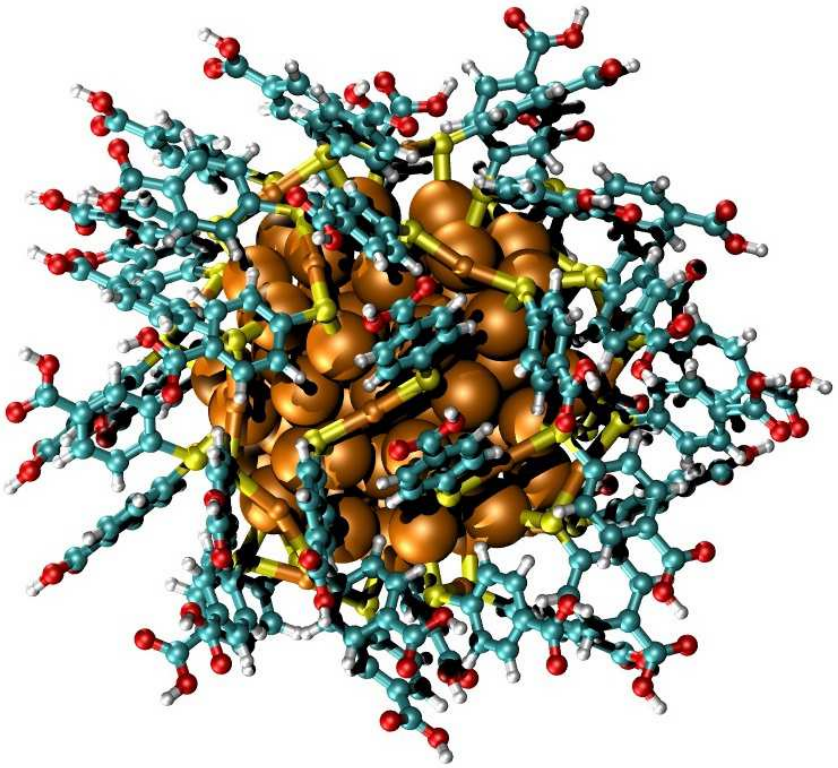

Figure 1. A presentation of the structure of $Au_{102}(p\text{MBA})_{44}$ cluster. Au atoms are in gold, C in turquoise, O in red, S in yellow, and H in white.
Courtesy of Sami Malola.

The structure of the gold core varies with the size of the particle.[19,33] In the larger particles (> 144 Au atoms), the core typically adopts an fcc structure of the metallic gold.[19] For smaller ones, the core structures have been found to be, for example, dodecahedral or icosahedral.[19,33] For example, the $Au_{102}$ species shown in Fig. 1 has a Marks decahedron based core of 79 gold atoms. In addition to nearly spherical clusters, a prolate shaped core has been observed, for example, for $Au_{38}$ and $Au_{130}$ species.[26,29] It has also been shown that in some cases, the choice of ligand molecule affects the size and geometry of the cluster.[24]

Clusters larger than $Au_{25}$ species are generally intrinsically chiral even if the ligand itself is achiral.[25,34] This is due to the arrangement of the protecting gold–sulfur motifs around the metallic core. The chiral isomers have been separated by chiral liquid chromatography and studied by CD spectroscopy for $Au_{40}(SC_2H_4Ph)_{24}$.[34] This property has been of interest for potential use in enantioselective catalysis.

### 2.3.3 Electronic properties

Many of the interesting features of clusters are intimately related to their electronic properties. The electronic energy level structure affects the stability of the cluster and determines, for example, the electron affinity and ionization energy of the cluster.[2,35] In addition, the optical and photothermal cluster properties depend on the electronic structure of the cluster.[36]

Atoms and small molecules have discrete energy states, while the metals have a continuum of electronic states with no energy gap between the valence and conduction bands.[1,2] Clusters represent a size-dependent intermediate form between these extremes. The evolution of metallic bands from the discrete energy states can be qualitatively understood by starting from discrete states of an atom and observing a gradually increasing density of electronic states as the number of atoms contributing to the electronic structure increases. As the density of states increases, the discrete states group to form bands, and the gap between occupied and unoccupied states vanishes to form a continuum of states.

In material science, the distinction between metallic, semiconductor, or insulating materials is generally done based on the size of the energy or band gap of the material.[2] The existence and non-existence of the energy gap between occupied and unoccupied states or a HOMO–LUMO gap can also be used to divide clusters into metallic gapless species and insulating or molecular species with an energy gap. The evolution of the density of electronic states and the distinction between different cluster sizes is shown in Fig. 2. On the borderline between the molecular and metallic behavior, the energy gap is small. In this case, electrons can be excited to the unoccupied states by the thermal energy. Therefore, for the cluster to show molecular behavior, the energy gap has to be large enough.

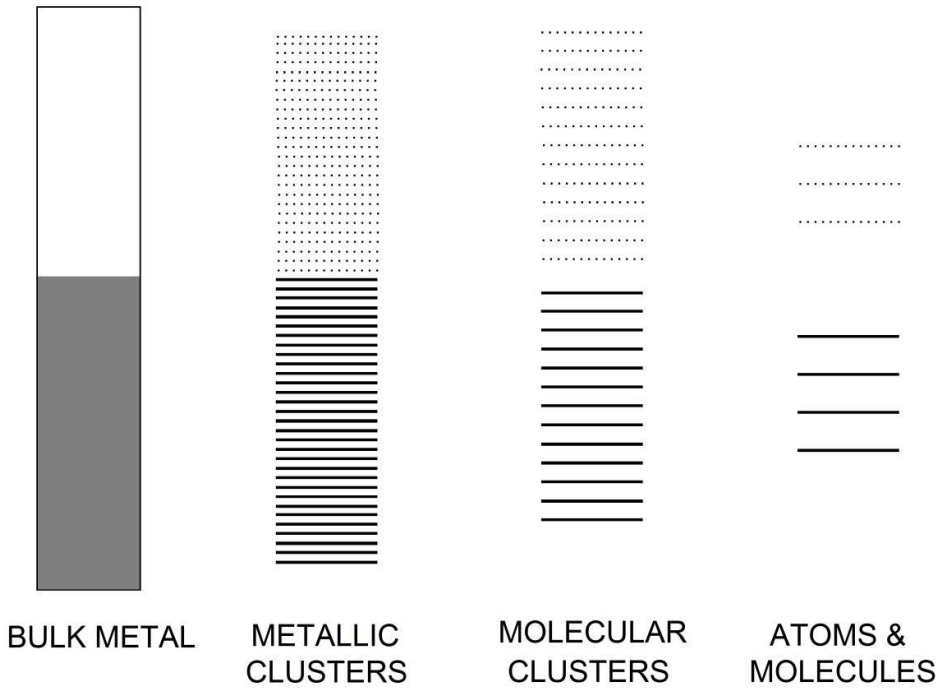


Figure 2. The effect of size on electronic structure of metal clusters. Picture adapted from ref. 2.

The difference between electronic state structure of clusters and bulk metals is induced by quantum confinement, which is the effect of limiting the electric field to small systems.[1,2,9] Several models can be utilized to study the electronic structure of clusters. The simplest model is the liquid drop model (LDM), which is a classic electrostatic model that considers the cluster as a conducting sphere.[2] LDM works well for the larger clusters and can be used to qualitatively describe trends for size-dependence of many cluster properties, such as ionization energies and melting temperatures.[2] Due to its classic nature, LDM fails to describe small clusters with diameters less than ~3 nm in which quantum size effects play a significant role.[2] The quantum effects can be taken into account by using the spherical jellium model in which the cluster is described as a positively charged sphere filled with electron gas.[2] For this system, the electronic energy states can be determined by utilizing an attractive potential induced by the core and using it to solve the Schrödinger equation. Other versions of the jellium model that are not limited to spherical geometry have also been developed.[37]

Another important feature of the electronic energy state structure of clusters is the formation of a shell structure.[2,35] Based on experimental[38] and computational results, it has been observed that the electronic states group into bands and form shells analogous to atomic structures. These types of shells are re-

ferred to as supershells. These results have led to the use of superatom theory, which will be described in more detail in the next section.[35]

For the small thiol-protected clusters with known structure, the electronic energy levels can be studied in more detail, since they can be calculated based on the specific cluster structure.[1,35,39] This type of study can be performed by utilizing DFT calculations, and can be used to explain experimental results accurately.[1,28,35,39,40] In the case of the ligand protected clusters, the ligand induced effects on the electronic levels have to be taken into account. For example, electronic states that are localized in the ligands or the interface are introduced to the system.

### 2.3.4 Stability and the superatom model

Stability of nanoclusters depends on the combined effect of cluster geometry and electronic properties.[2,35] For small clusters, the electronic effects generally dominate due to increased importance of quantum mechanical effects, while the geometric effects are more important for larger particles. The increased stabilities of certain cluster sizes has led to a concept of magic numbers, a sequence of numbers indicating particularly stable cluster sizes.

As stated in the previous section, the electronic levels of the clusters form bands, which in turn form supershells.[35] This type of concept is analogous to electronic shells of atoms and is used in the superatom theory. In this theory, the bands of states of clusters are treated as superatom orbitals, and in analogy to atoms, the most stable species correspond to the shell closings. According to the model, the lowest energy superatom orbitals, which are mainly derived from gold 6s orbitals are $1S^2|1P^6|1D^{10}|2S^21F^{14}|2P^61G^{18}|2D^{10}3S^21H^{22}|\ldots$, where the letters indicate the angular-momentum characters. Based on this, the magic numbers are 2, 8, 18, 34, 58, 92, 138….

For the thiol protected clusters, the stability consideration and the number of electrons is affected by the ligand layer and the electron withdrawing nature of the thiol ligands. The magic numbers for these clusters can be described by utilizing the divide and protect model for the structure of the clusters.[35] The electron counting rule for the protected clusters is shown in equation (1).

$$n^* = Nv_A - M - z, \quad (1)$$

where $n^*$ is the shell-closing electron count of the metallic core, $N$ is the number of core atoms, $v_A$ is the atomic valence, $M$ is the number of electron withdrawing monodentate ligands, and $z$ is the overall charge of the cluster.

Stable thiol-protected clusters that do not follow the above mentioned magic numbers have also been observed.[31] This indicates that for certain cluster sizes, the geometric effects are important even though the cluster is relatively small. Recently, it has also been shown that the ligand can also affect the size and geometry of the gold core.[24]

### 2.3.5 Optical properties

The first application of colloidal gold particles, which have been used for centuries, has been their use as red pigment in stained glass.[1] This example demonstrates the unique optical properties of the particles compared to bulk properties. Since the optical properties of clusters are closely related to their electronic properties, quantum confinement and the density of electronic states play a significant role.[1-2,9,41] When studying the optical features of the clusters, a division between small clusters and larger species is important, since the optical response of the clusters in different size regions is also different.

The most interesting and most prominent optical feature supported by the larger gold nanoclusters is the localized surface plasmon resonance (LSPR).[9,12,42] The LSPR is a collective charge density oscillation of the conduction electrons that are localized on the surface of metals. [9,12,42] LSPR is responsible for strong scattering of light and also dominates the absorption spectrum of gold clusters with a single intense peak at ~530 nm. This absorption is responsible for the red color observed for the clusters. In addition, LSPR causes field-enhancement of the local electromagnetic fields. The plasmonic species have attracted tremendous interest in recent years, and the study of plasmons has broadened into its own research field. LSPR is also very attractive for various applications including sensors that are based on the field-enhancement effects.[12]

For small clusters with a significant energy gap, no plasmon band is observed and the optical properties reflect the electronic energy structure of the system.[1,28,40] The clusters generally show strong absorption. Due to the fact that electrons can be optically excited from the occupied states to the unoccupied states and due to the relatively large density of electronic states, the cluster spectrum is generally continuous with features characteristic to the specific band structure of the cluster. Because of the continuous spectrum in the visible range, the clusters appear black or brown.

### 2.3.6 Molecular and metallic behavior

As mentioned in Section 2.2, clusters are in many contexts divided to molecule-like and metallic particles based on their size, and one of the general research questions in cluster studies is to determine the exact number of atoms required to induce the transition from molecular to metallic behavior.[2] This question has been addressed for gold by using different methods and also for different type of samples.[41-45] In addition, different types of criteria for molecular and metallic behavior based on the electronic and optical cluster properties have been used.[41-45] The results of some of these studies are briefly discussed here together with the criteria and methods used in the work presented in this thesis.

The evolution of the metallic electronic energy bands has been studied in the gas phase for a large number of mass selected clusters.[44] The results show discrete absorptions for the smallest clusters with sizes up to few tens of atoms. For larger sizes, formation of the d-band and the sp-band typical for bulk met-

als is clearly seen. On the other hand, the energy gap closing has been studied by STM for two-dimensional clusters on MgO on Ag surface.[45] For these clusters, the gap closing was found to occur between 70 and 100 gold atoms. Another possibility to characterize the metallic nature is to study the geometry of the gold core and the evolution of the structure towards the fcc lattice.[19] For thiol-protected clusters, the $Au_{144}$ species has shown to be the largest cluster with molecular arrangement of core atoms with an icosahedral core. In the same study, the $Au_{187}$ species was shown to have a core with the fcc lattice indicating that the transition region is somewhere between these cluster sizes. The emergence of the plasmon band can also be used as a criterion for metallic behavior.[41,42] Based on computational results, the metallic LSPR band is observed for clusters larger than the $Au_{144}$ species.[42]

For the purpose of the work presented in this thesis, the crucial property used to define the molecular or metallic behavior is the existence of electronic energy gap or a HOMO–LUMO gap. One of the techniques that can be used to determine the existence of the gap is transient absorption spectroscopy.[27,36,43,46–54] Recently, the transition from molecular to metallic behavior for monodisperse samples of the ligand-protected clusters has been of great interest, and the work presented in this thesis is part of this effort.[I-III] Based on transient absorption studies, Varnavski et al.[54] narrowed the molecular behavior to cluster size of about 2.2 nm, which corresponds to ~300 atoms. The small gold clusters with 11, 25, and 28 atoms have been identified as molecular.[48–53] In other studies, $Au_{102}$, $Au_{115}$, $Au_{117}$, and $Au_{133}$ species have been shown to present non-metallic behavior,[27,47] while the $Au_{144}$ cluster has been identified as a metallic species.[46,47] For phosphine protected clusters, the transition between different behaviors has been indicated to occur between 13 and 55 gold atoms.[43] The use of transient absorption in clusters studies is described in more detail in Section 2.5.8.

### 2.3.7 The ligand layer

The protecting ligand layer has an effect on the cluster structure, and its electronic and optical properties as presented in previous sections. In addition, the ligand molecules are responsible, in particular, for many of the chemical properties of protected clusters, since the ligand layer is directly in contact with the surrounding environment. Hence, the ligand layer has to be taken into account when handling the cluster samples. For example, the solubility of the clusters to different solvents depends on the ligand molecule and its protonation state.[55] The ligand layer and the protecting units have not been studied as widely as the gold core, but for example, vibrational and NMR spectroscopy have been used in their studies.[40,56–58]

The ligand layer also offers versatile possibilities for utilizing the clusters in applications, since the ligand layer can be modified chemically to achieve desired functionality. It has been shown, for example, that by utilizing a ligand

exchange reaction, the ligands of existing clusters can be changed into other molecules.[59] One example of chemical modification has been presented by Marjomäki et al., who modified the ligand layer of *p*MBA protected clusters to include a linker molecule that can selectively be attached to cysteine residues on a surface of a virus.[60]

## 2.4 Studied clusters

In the work presented in this thesis, three clusters with different sizes were studied.[I–III] These clusters were $Au_{102}(pMBA)_{44}$, $Au_{144}(SC_2H_4Ph)_{60}$, and a previously unreported cluster tentatively identified as $Au_{130}(pMBA)_{50}$. The structure and some previously reported electronic properties of the clusters are briefly discussed in this chapter.

These clusters were primarily chosen based on their size, which falls into the size region close to the expected transition region between molecular and metallic behavior. For the first two studies presented in papers I and II, well known stable cluster compositions were chosen to accurately link the photodynamics of the system to a particular structure and also to previously obtained results. In addition, the synthetic procedure of the cluster also had to be well established to produce large enough quantities of the highly monodisperse sample for the performed experiments. Following the work presented in papers I and II, an intermediate cluster size was chosen to bridge the region between the previously studied cluster sizes.

### 2.4.1 $Au_{102}(pMBA)_{44}$

The $Au_{102}(pMBA)_{44}$ cluster has been a subject of many studies since the determination of its structure, which is shown in Fig. 1.[25] The cluster is composed of a $Au_{79}$ core protected by 19 S–Au–S units and two S–Au–S–Au–S units. The cluster is stable, and it can be understood as a superatom complex for electronic shell closing of 58 electrons.[35] Based on electronic structure calculations and experimental electronic spectrum, the $Au_{102}$ species has a HOMO–LUMO gap of 0.45 eV, indicating a molecular behavior.[40] It has also been shown that the cluster is water-soluble in partly deprotonated form.[55]

### 2.4.2 $Au_{144}(SC_2H_4Ph)_{60}$

The exact cluster composition for the $Au_{144}$ species has been determined by mass spectrometry studies,[17] but the exact structure of the cluster has not been determined despite active effort.[61] However, a widely accepted model for the structure has been proposed based on DFT calculations.[61] The proposed structure includes an icosahedral $Au_{114}$ core protected by 30 S–Au–S units.[61] A

presentation of the structure based on this model is shown in Fig. 3. Based on calculations[61] and electrochemical experiments,[62] the cluster has no HOMO–LUMO gap, thus indicating metallic behavior. However, the cluster has been shown to have an optical gap of ~0.27 eV due to selection rules.[56,63]

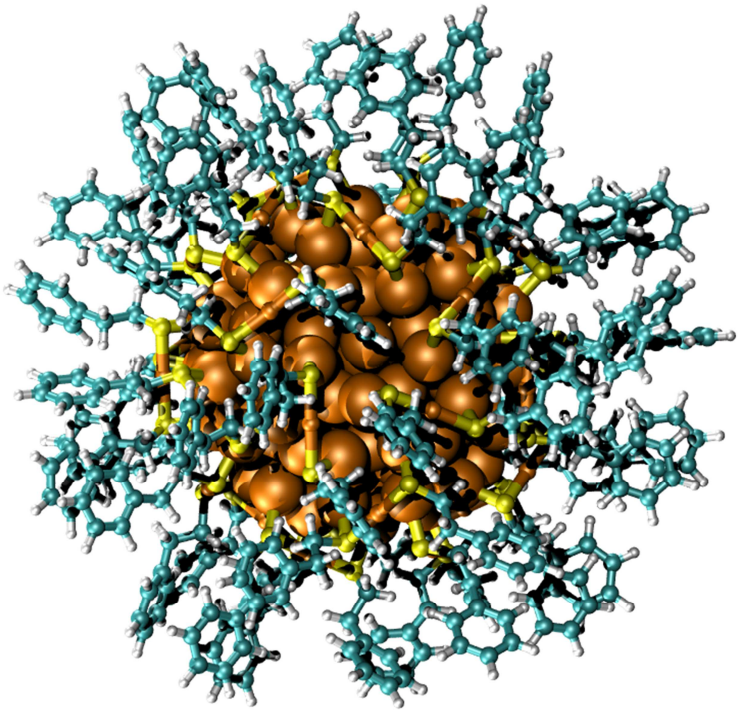

Figure 3. The proposed structure of $Au_{144}(SC_2H_4Ph)_{60}$ cluster. Courtesy of Sami Malola.

### 2.4.3 Clusters with $Au_{130}$ core

$Au_{130}(SR)_{50}$ was first introduced when the species was isolated by chromatography and identified by mass spectrometry.[31] After that, clusters with $Au_{130}$ core have been reported with different organosoluble ligands.[23–24,26,64] Tsukuda and Negishi also proposed a structure of the cluster, which was later confirmed by calculations to be reasonable.[31,65] Recently, the proposed structure was also confirmed by x-ray crystallography.[26] The structure of the cluster core is slightly prolate shaped and closely resembles the structure of the core of the $Au_{102}$ cluster.[26,31] The optical spectrum of these organosoluble clusters has been reported and shows no significant plasmon band, but no detailed study of the energy gap magnitude has been reported. Electrochemical studies for this cluster size indicate non-molecular behavior.[66]

## 2.5 Optical spectroscopy and its utilization in cluster studies

### 2.5.1 The spectrum of electromagnetic radiation

Light is a form of electromagnetic radiation. Classically it can be understood as perpendicular oscillating electronic and magnetic fields. Due to wave-particle duality light can also be described by photons. The energy of the electromagnetic radiation and the photon depends on the wavelength of the radiation according to equation (2).[3,4]

$$E = \frac{hc}{\lambda}, \tag{2}$$

where $E$ is the photon energy, $h$ is the Planck constant, $\lambda$ is the wavelength of the radiation, and $c$ is the speed of light.

The full spectrum of electromagnetic radiation spans over a wide wavelength range, which is generally divided into different parts based on the use and effects of the radiation.[3,4] The full spectrum includes different regions from low energy radio frequencies and microwaves to higher energy visible light and high energy x-rays and cosmic rays. The spectrum of electromagnetic radiation as a function of wavelength is shown in Fig. 4.

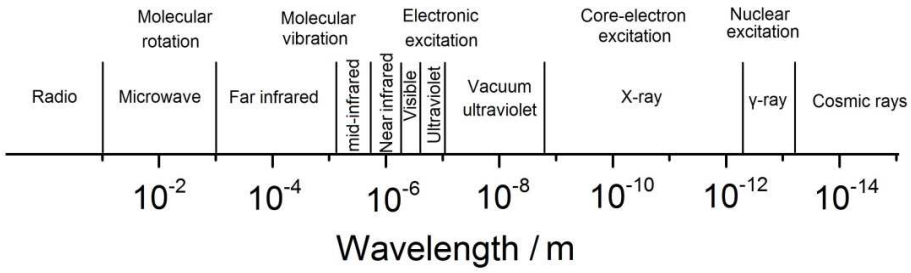


Figure 4. Different regions of the electromagnetic spectrum. The interaction of different regions with molecules is shown above the wavelength regions.

### 2.5.2 Spectroscopy and hierarchy of energy levels in molecules

Spectroscopy considers the interaction between light and matter including absorption, scattering, and emission processes.[3,4] The light and matter interaction is mainly mediated by the electric field component of the light. A spectroscopy measurement generally includes the study of the interaction of light as a function of wavelength. This type of experiment can be used to access information about the energies required to transfer the system between different energy states. Different regions of the electromagnetic spectrum have a different type

of effects on the samples and utilization of various spectral regions yields information on different properties of the sample. These interactions in different wavelength regions with molecules are shown in Fig. 4.

The interaction between different wavelengths regions of light and molecules is induced by a hierarchy of energy levels in molecules.[3,4] The electronic energy levels of molecules are determined by the structure of the molecule and the electronic states of the individual atoms. Each electronic state is associated with it several possible vibrational states, which in turn have several rotational states that are relevant in the gas phase. The energy required for vibrational or rotational transition is, therefore, significantly smaller than the energy required for electronic excitation. The work presented in this thesis concentrates on electronic excitation in the visible and near infrared regions and on vibrational modes of the clusters in the mid-IR region.

### 2.5.3 UV/vis spectroscopy

The radiation in the UV/vis region generally matches the differences between electronic energy levels in the molecules.[3,4] Therefore, electronic energy levels and molecular properties related to the electronic structure can be studied by this method. The absorption spectrum in this region can be obtained by measuring the intensity of light at different wavelengths with and without the sample. The amount of light absorbed by the sample is usually determined by absorbance, which can be calculated according to equation (3). The second part of equation (3) shows how the absorbance value depends on the sample concentration and optical path of the sample. This part is known as the Beer–Lambert law.[3,4]

$$A = log \frac{I}{I_i} = \varepsilon cl, \tag{3}$$

where $A$ is the absorbance, $I$ is the transmitted intensity, $I_i$ is the intensity entering the sample, $\varepsilon$ is the molar absorption coefficient of the sample, $c$ is the sample concentration, and $l$ is the optical path length of the sample.

The spectrum can be measured by using a UV/vis spectrometer, a device designed for absorption experiments in this region. A schematic presentation of the measurement is shown in Fig. 5.

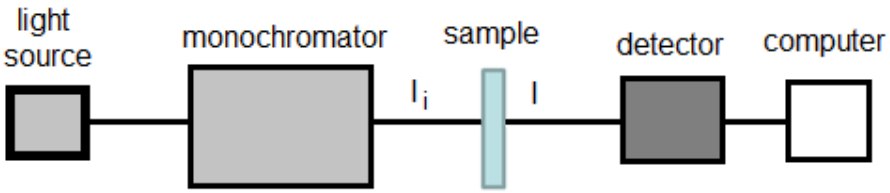


Figure 5. Schematic presentation of a UV/vis spectrometer.

### 2.5.4 Infrared spectroscopy

Molecules are in constant vibrational motion and have several vibrational modes depending on the number of atoms.[3,4] Since the vibrational modes of many functional groups are highly localized, IR spectrum can be used to identify these groups in molecules. Infrared spectrum can also be used to identify the sample, since the spectrum is characteristic for each molecule. Due to selection rules, only the vibrational modes that induce a change in the dipole moment of the sample can be studied by this method.

In addition, the IR spectroscopy can be used to obtain versatile information, for example, about the vibrational energy level structures and anharmonicity of the vibrational modes. [3,4] Since populations of different vibrational energy states depend on temperature according to the Boltzmann distribution, changes in the peak positions and widths can be used to analyze the effects of temperature in the system.

Measurement of an IR spectrum is generally done by using a FTIR spectrometer, a device based on a Michelson interferometer. In this technique, the spectrum is first measured in a time domain as an interferogram and then calculated in frequency domain by using a Fourier transformation. A schematic presentation of an FTIR spectrometer is shown in Fig. 6.

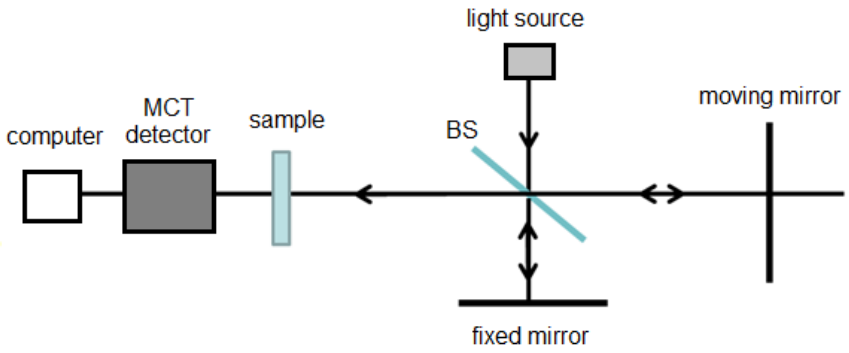


Figure 6. Schematic presentation of an FTIR spectrometer.

### 2.5.5 Electronic and vibrational spectroscopy in cluster studies

UV/vis spectroscopy can be used to study the electronic properties of the clusters. For large plasmonic clusters, the plasmon absorption dominates the UV/vis spectrum with a single strong and broad absorption at ~530 nm.[1,2,41] Due to the strong plasmon peak, UV/vis spectrum can also be used to study the existence or non-existence of a plasmon band and, therefore, used to estimate the molecular or metallic behavior of the cluster. Since the optical properties of small non-plasmonic clusters depend on the electronic properties of the cluster, the spectrum can also be used in sample characterization for these cluster sizes.[1, 17,40] Due to the high density of states in the clusters, the optical spectra of the clusters generally show broad continuous absorption in the entire UV/vis region. By comparing the experimental spectra with computational results, the different spectral features can be identified in more detail.[19,28,40] As an example, the UV/vis spectrum of $Au_{102}(p\text{MBA})_{44}$ is shown in Fig. 7.

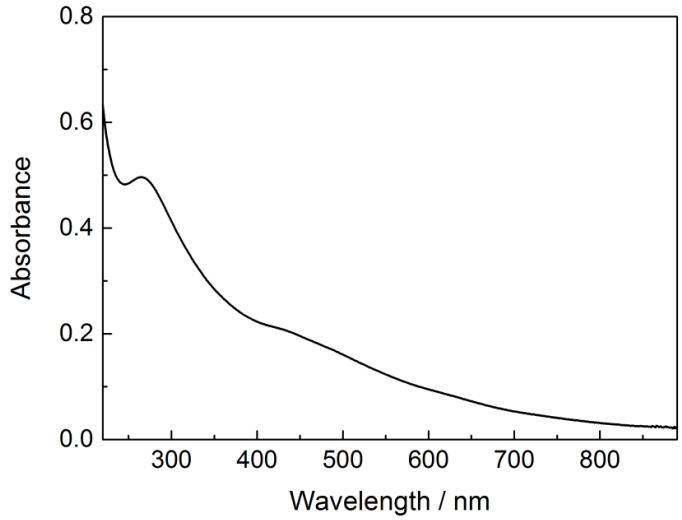


Figure 7. UV/vis spectrum of $Au_{102}(p\text{MBA})_{44}$.

The vibrational modes of the clusters in the mid-IR region are mainly localized in the ligand molecules.[40,56,63] Therefore, the studies in this region are generally concentrated on the ligands. To study the vibrational modes of the Au–S interface, far-IR spectroscopy can be used.[67] In addition, the onset for electronic absorbance of the clusters can be studied in this region for many cluster sizes.[40,56,63]

### 2.5.6 Time-resolved spectroscopy

To understand energy relaxation processes occurring after the electronic excitation, it is useful to study the time dependence of sample properties. Time can be

added as another dimension in spectroscopy experiments by using pulsed light. The time scale in which nuclear motion and molecular relaxation of the atoms occur is in the femtosecond to picosecond range ($10^{-15}$–$10^{-12}$ s).[5] Therefore, femtosecond pulses can be utilized to study molecular relaxation and photochemical reactions in time scale relevant to molecules. This type of pulses in different spectral regions can be obtained by using pulsed lasers.[68,69] To understand the time resolved experiments and their results, different electronic relaxation processes and the role of different energy states in the relaxation must be understood. These are discussed below.

#### 2.5.6.1 Electronic excitation and relaxation

When a photon with energy matching the energy difference between two electronic states of the sample interacts with a sample system, the photon can be absorbed and electronically excite the sample.[3,5] Depending on the electronic energy state structure of the molecule, the excess energy provided by the photon can induce different relaxation processes and photochemical reactions. Following the excitation, the molecule relaxes back to its electronic ground state or to photoproducts. Different relaxation processes depend on the electronic energy structure of the molecule and can be non-radiative or radiative. The initial excitation energy can be lost as heat, emitted photons, or be used to form photoproducts. The existence or non-existence of the HOMO–LUMO gap also has a significant role in the relaxation processes, and the time scales of relaxation can vary several orders of magnitude between molecular and metallic systems.

#### 2.5.6.2 Molecular systems

For molecules, the electronic relaxation can be generally understood by single electron excitation and subsequent electronic and vibrational relaxation processes.[5] Following an absorption of a photon, the molecule is generally excited to higher energy electronic state with the same spin state as the ground state. Most commonly, this is a singlet state. The molecule also generally has excess vibrational energy in the electronic state. The relaxation back to the electronic ground state (GS) can occur via different pathways. In each of the electronic states, the energy can relax via vibrational relaxation (VR) towards the minimum vibrational energy of the state. In addition, the molecule can change its electronic state to lower energy states with different spin states. Non-radiative transition between electronic states having the same spin is called internal conversion (IC), while the formally forbidden transition between different spin states is referred to as intersystem crossing (ISC). For molecules, the ISC generally occurs between singlet and triplet manifolds. Once the molecule is relaxed to the lowest excited state, it can return to the ground state by emitting a photon. The emission from the states with the same spin state is called fluorescence (FL), while the transition from a state with different spin is called phosphorescence

(PH). The relaxation via the forbidden transitions is generally long-lived when compared to the allowed transitions. Due to a HOMO-LUMO gap in molecules, the radiative relaxation either as fluorescence or as phosphorescence is a common phenomenon. Typical time scales for the different relaxation processes vary from sub-picosecond IC for high energy electronic states and picosecond scale for vibrational cooling to nanoseconds for fluorescence from lowest excited states. The spin forbidden radiative relaxation from a different manifold of spin states is generally slower than fluorescence and may occur even in seconds or minutes.

The relaxation processes in molecules are generally described by Jablonski diagrams, which show the electronic energy states as lines and different processes as arrows. This kind of presentation is shown in Fig. 8. Alternatively, the electronic states of the system can be presented as potential energy surfaces.

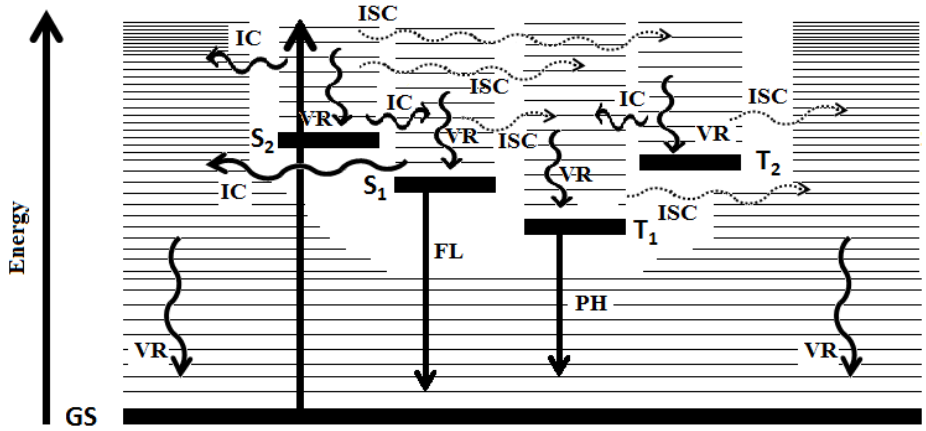


Figure 8. The relaxation processes involving singlet and triplet manifolds of molecular systems presented as a Jablonski diagram. The thinner lines represent the vibrational energy levels of the molecule. See text for description of various processes.

### 2.5.6.3 Metallic systems

For metallic systems, there is no significant energy gap. This facilitates a different type of relaxation compared to molecular systems.[36] In metals the excitation energy is first rapidly distributed via electron-electron scattering. In this process, the energy is non-thermally distributed between electrons to create a hot electron distribution corresponding to high temperatures. This process generally occurs in the femtosecond time scale. Due to electron-electron scattering, the information about the original excitation is rapidly lost. Subsequently, the energy is transferred to vibrational motions of the atoms via electron-phonon coupling. The efficiency of this coupling is determined by the electron–phonon

coupling constant, and it affects the relaxation time. Finally, the energy is dissipated into the surrounding medium via collisions. With this type of metallic relaxation, the energy of the photon is efficiently converted to heat, since there is no significant relaxation via emission.

#### 2.5.6.4 The two-temperature model

The photothermal behavior of metals after electronic excitation by light has been studied for a long time and can be successfully explained by the so-called two temperature model.[36,46,47,70] The model describes heat transfer from the optically excited electrons to the unexcited metallic lattice. In this model, two coupled differential equations (4a–b) can be used to describe the energy flow from the excited electrons to the lattice.

$$C_e(T_e)\frac{dT_e}{dt} = -g(T_e - T_l) \quad (4a)$$

$$C_l\frac{dT_l}{dt} = g(T_e - T_l) \quad (4b)$$

$$C_e(T_e) = \gamma T_e \quad (4c)$$

In these equations, $C_e$ and $C_l$ are the heat capacities of the electrons and the lattice, respectively, $g$ is the electron-phonon coupling constant, and $\gamma$ is a constant, which for gold is $\gamma$ = 66 J m$^{-3}$ K$^{-2}$.[46] The electronic heat capacity depends linearly on the temperature as shown in equation (4c). Because the heat capacity of the excited electrons is temperature-dependent, the rate of heat transfer depends on the excitation energy. This kind of behavior can be used as an indication of metallic behavior in the clusters and can also be used to determine the electron–phonon coupling constant for the cluster. Generally, the electron-phonon coupling constant is determined by using low excitation energies[71] or by measuring the relaxation time of the system with different excitation energies and then extrapolating the results to zero energy.[36,46,47]

### 2.5.7 Transient absorption spectroscopy

Transient absorption spectroscopy can be used to obtain a time-dependent absorption spectrum of the sample by utilizing pulsed light.[4,68,69] This type of experiment can be used to study especially the non-radiative photochemical and photophysical properties of the systems.

Transient absorption experiment is a pump–probe measurement in which the sample is first excited by a pump pulse. [4,68,69] The changes induced by the pump pulse are then monitored by a probe pulse, which is detected. Time dependence can be introduced to the experiment by delaying the probe pulse with respect to the pump pulse by modifying the distance travelled by the beams

and repeating the measurement with several time delays. This is done by using a movable delay line. A schematic presentation of a transient absorption measurement is shown in Fig. 9.

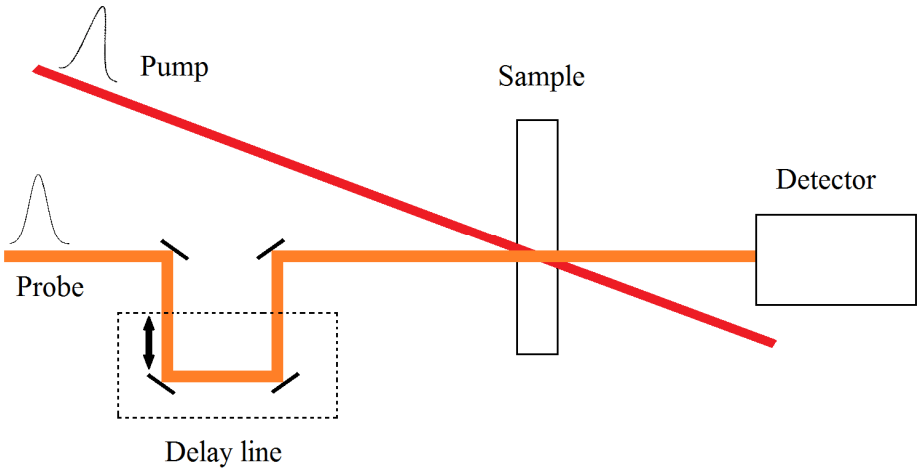


Figure 9. A schematic presentation of a transient absorption experiment.

Transient absorption spectrum is generally presented as a difference spectrum between sample absorption with and without excitation. The transient absorption signal can then be calculated as shown in equation (5).

$$\Delta A[OD](\lambda, \Delta t) = log \frac{I_0(\lambda)}{I(\lambda,\Delta t)_{excitation}} - log \frac{I_0(\lambda)}{I(\lambda,\Delta t)_{no\ excitation}} \quad (5)$$

where $I_0$ is the intensity entering the sample and $I_{excitation}$ and $I_{no\ excitation}$ are the intensities transmitted with and without excitation. To improve the shot-to-shot signal to noise ratio, the probe beam can be split into two separate beams that enter the sample at different spots and are detected separately. This type of method allows simultaneous measurement of intensities with and without excitation.

The transient signal includes positive and negative features when the absorbance of the sample is increased or decreased after the excitation. The changes in absorbance can be due to the ground state bleach, stimulated emission, excited state absorption, or by photoproduct absorption. In general, no signal is observed when the probe pulse enters the sample before the pump pulse. However, in the mid-IR region a non-zero transient signal is sometimes observed. This signal is induced by perturbed free induction decay, which is a coherent effect that is observed when the time resolution of the experiment is shorter than the phase relaxation of the vibrational transition.[72]

To obtain information about the photodynamics of the sample, the obtained time dependent absorption signal needs to be analyzed. The relaxation

time constants for different relaxation processes can be obtained from the data by fitting. In many cases, the signal decays exponentially and a sum of exponential components is fitted to the data to extract the time constants for different processes. The fitting is done according to equation (6).

$$\Delta A[OD](\lambda, \Delta t) = \sum_i^n A_i(\lambda)\exp(-\Delta t/\tau_i), \qquad (6)$$

where $A_i$ is the amplitude of component $i$, $\Delta t$ is the time delay, and $\tau_i$ is the relaxation time constant of component $i$.

### 2.5.8 Transient absorption in nanocluster studies

Larger plasmonic clusters with different cluster sizes have been studied extensively by UV/vis region transient absorption experiments.[36] Relaxation dynamics typical for metallic systems have been observed for these clusters. In addition, the two temperature model has been used to extract the electron–phonon coupling constants for the clusters based on the excitation energy dependence of the recovery of plasmon bleach band absorption.

The use of transient absorption experiments in determining the molecular and metallic behavior was already mentioned in Section 2.3.6. The use of this method for this purpose is based on the differences in the relaxation time scales in molecular and metallic systems described in Sections 2.5.6.2 and 2.5.6.3. Generally, fast relaxation in time scale of a few tens of picoseconds has been observed for metallic species, while the relaxation of molecular clusters extends to hundreds of picoseconds or even nanoseconds.[27,36,43,46–54] In addition, the excitation fluence dependence or independence based on the two temperature model has been used as an indicator of metallic or molecular behavior.[27,46,47]

The UV/vis region transient absorption of $Au_{25}$ species has been studied rather extensively by several groups in anionic and neutral form and also in rod shaped form.[48–51] The relaxation dynamics of this species was observed to depend on the charge state of the cluster. Some relaxation processes were also interpreted. These processes involve the initial relaxation from the excited state to lower exited states referred to as semi-ring states, which are localized in the protecting gold-sulfur units, and radiative relaxation to the ground state.

In addition to UV/vis region transient absorption, mid-IR region probing has been used for studying energy transfer from gold clusters to protein capping layer and villin capped clusters.[21,22] Based on these studies, it has been shown that the energy introduced to the clusters as electronic excitation is transferred to heat and proceeds in the protein chain in the form of vibrational energy[22], and that the protein folding of villin is not affected by the laser induced heating of the system.[21]

# 3 EXPERIMENTAL METHODS

## 3.1 Samples and sample characterization

The studied cluster samples were $Au_{102}(p\text{MBA})_{44}$, $Au_{144}(SC_2H_4Ph)_{60}$, and a previously unreported cluster identified as $Au_{130}(p\text{MBA})_{50}$. $Au_{144}(SC_2H_4Ph)_{60}$ and $Au_{102}(p\text{MBA})_{44}$ samples were synthesized according to previously published procedures.[17,55] The $Au_{130}$ species was obtained as a by-product of $Au_{102}(p\text{MBA})_{44}$ synthesis[57] and was isolated by a separate precipitation procedure explained in detail in paper III. All cluster samples were obtained via an in-house collaboration.

For the performed studies, it is important to know the sample composition, and to confirm the high monodispersity of the samples. Therefore, composition and the monodisperse nature of all samples were first studied with several methods. In each case, the sample was characterized by UV/vis and infrared spectroscopy together with NMR spectroscopy.[73] In addition, composition of the organosoluble $Au_{144}$ sample was confirmed with mass spectrometry.[73] For the water-soluble *p*MBA protected clusters, size and monodispersity of the sample were confirmed by SDS-PAGE analysis.[II-III] In each analysis, the results of used samples were compared to a reference for monodisperse samples and also compared to computational results when possible.

## 3.2 Sample preparation and handling

All clusters were studied in solutions. The solvents were mainly chosen based on the solubility of the sample and on the solvent IR spectrum. High enough solubility of the sample was needed to allow high cluster concentrations, and the solvent IR spectrum was required to provide a suitable transparent window to allow the sample absorption to be monitored. In the experiments the organosoluble $Au_{144}(SC_2H_4Ph)_{60}$ cluster was dissolved in deuterated dichloromethane (DCM-D2), while the *p*MBA-protected clusters were dissolved in $D_2O$.[I-III]

It has been shown that in a $D_2O$ solution, the carboxylic acid groups of the *p*MBA ligands are partly in deprotonated form and that the immediate surrounding solvent layer depends on the counter cation.[55] In addition, the cluster is insoluble in methanol.[18,55] In the present work, $Na^+$ was used as the counter cation in all solutions. The cations can be incorporated to the cluster sample by precipitating the sample in deprotonated form from a water-methanol mixture. $Na^+$ counter cation can be obtained by using NaOH to precipitate the sample. Before the spectroscopic measurements the sample was dried and then dissolved in $D_2O$. Since it was shown that the dichloromethane solution of cluster samples can be contaminated if it is in frequent contact with polymeric labware[63], special care was taken to avoid sample contamination of the $Au_{144}(SC_2H_4Ph)_{60}$ solution by only using materials suitable for chlorinated solvents when handling the solution.

## 3.3 Spectroscopy studies

Transient absorption was chosen as the research method to study the photodynamics of the clusters. Visible and NIR light was chosen for pumping to electronically excite the cluster core, and the mid-IR region was chosen for probing to obtain information about the vibrational relaxation and to monitor the energy flow from the initially excited gold core to the ligands. Due to the drastically different relaxation time scales for molecular systems and gapless metallic systems, transient absorption method is also well suited for the distinction between molecular and metallic cluster behavior as stated in Section 2.5.8. Since the time scale of the relaxation dynamics is highly dependent on the existence of the energy gap, transient absorption is a sensitive and relatively straightforward method for this type of studies. In previous studies, the existence and magnitude of the energy gap has been determined by linear spectroscopy.[40,56,63] However, the determination of the onset for electronic absorbance is hindered by the broad absorption bands of the clusters and the weak electronic absorbance close to the gap. This type of difficulty in using the linear spectra in the determination of the existence of the gap was also observed for the studied $Au_{130}$ species.[III]

Prior to the photodynamics studies each cluster sample was characterized by UV/vis and FTIR spectroscopy. For the electronic spectrum measurements a 1 mm optical path quartz cuvette was used. The measurements in the mid-IR region were performed in a flow cell[74] with an 80 μm optical path length. The solvent absorption was removed from all measured spectra by subtraction.

The transient absorption experiments were performed by using a home-built UV/vis pump–mid-IR probe spectrometer. The used laser setup is based on a Ti:Sapphire amplifier from which ~100 fs laser pulses at ~800 nm are obtained with a 1 kH repetition rate. The mid-IR beam used for probing is generated from the fundamental beam by using a double-pass optical parametric amplifier (OPA) combined with difference frequency mixing of the signal and

idler beams from the OPA.[75] Before the sample, the beam is divided into a probe and a reference beam, which enter the sample in different spots and are detected separately. The detection is done by using a double array MCT (HgCdTe) detector. The pump pulse is produced from the fundamental beam by using a TOPAS device (travelling-wave optical parametric amplification of superfluorescence) and is aligned to hit the sample at the same spot as the probe beam. Every second pump pulse is blocked by a synchronized chopper. The time resolution of the experiment was determined by the rise time of electron signal in thin silicon wafer and was found to be ~250 fs. A schematic representation of the used setup is shown in Fig. 10, and a more detailed description of the used laser setup is described in Ref. 76.

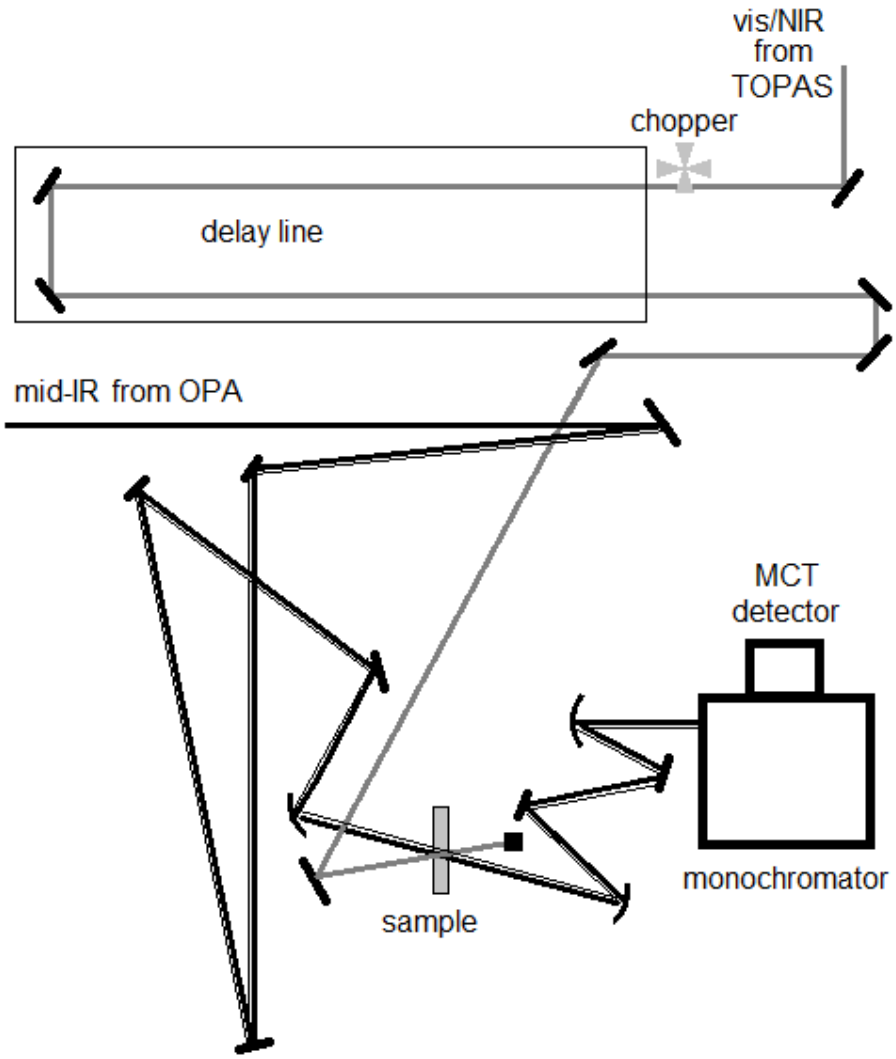


Figure. 10. A schematic presentation of the transient absorption setup used in the experiments. The pump is shown in gray and the probe in black. The thinner black line represents the reference beam.

The sample solution was moved back and forth in the flow cell[74] by utilizing a microfluidic flow controller system during each measurement to prevent laser induced sample damage. This technique also facilitated the measurements to be performed with small sample volumes, since only 50–100 µl of sample solution was used. The transient spectrum for each sample was measured by averaging at least five spectra to improve the signal-to-noise ratio. In addition, different excitation energies were used to determine the pump fluence dependence of the transient absorption spectrum of the samples.

# 4 RESULTS AND DISCUSSION

The main results of the work reported in papers I–III are presented and discussed in this chapter. For each of the studied clusters, the results of spectroscopic characterization obtained by electronic and vibrational spectroscopy are shown in addition to the results of the photodynamics studies. Finally, the results for different particle sizes are combined to address the transition from molecular to metallic behavior of gold clusters, and to discuss the implications of the results.

## 4.1 $Au_{144}(SC_2H_4Ph)_{60}$[I]

The UV/vis spectrum and the molar absorption coefficients of the $Au_{144}$ species are shown in Fig. 11A. The spectrum nicely matches with the previously reported spectrum, thus partly confirming the quality of the sample.[17] The spectrum clearly shows strong continuous absorption from the NIR to UV region with no significant plasmon band. FTIR spectra of both the sample and the ligand molecule measured in DCM-D2 solution are shown in Fig. 11B. It can be seen that the vibrational spectrum of the cluster closely resembles that of the PET (PET= phenylethanethiol) ligand. This result is reasonable since the vibrational modes of the cluster in this region are expected to be highly localized on the ligands. The comparison between the spectrum of PET and $Au_{144}$ species also shows that the absorption band induced by the S–H stretching vibration in PET, which is observed at ~2600 $cm^{-1}$, disappears for the cluster, thus indicating the formation of the Au–S bond. In addition to the absorption of the vibrational modes, electronic absorption can also be seen from the FTIR spectrum as continuously rising absorption in the higher energy region of the spectrum. The onset of the electronic absorption is observed at ~2200 $cm^{-1}$ and is marked with a red arrow in Fig. 11B. This result also matches nicely with previously reported results.[63]

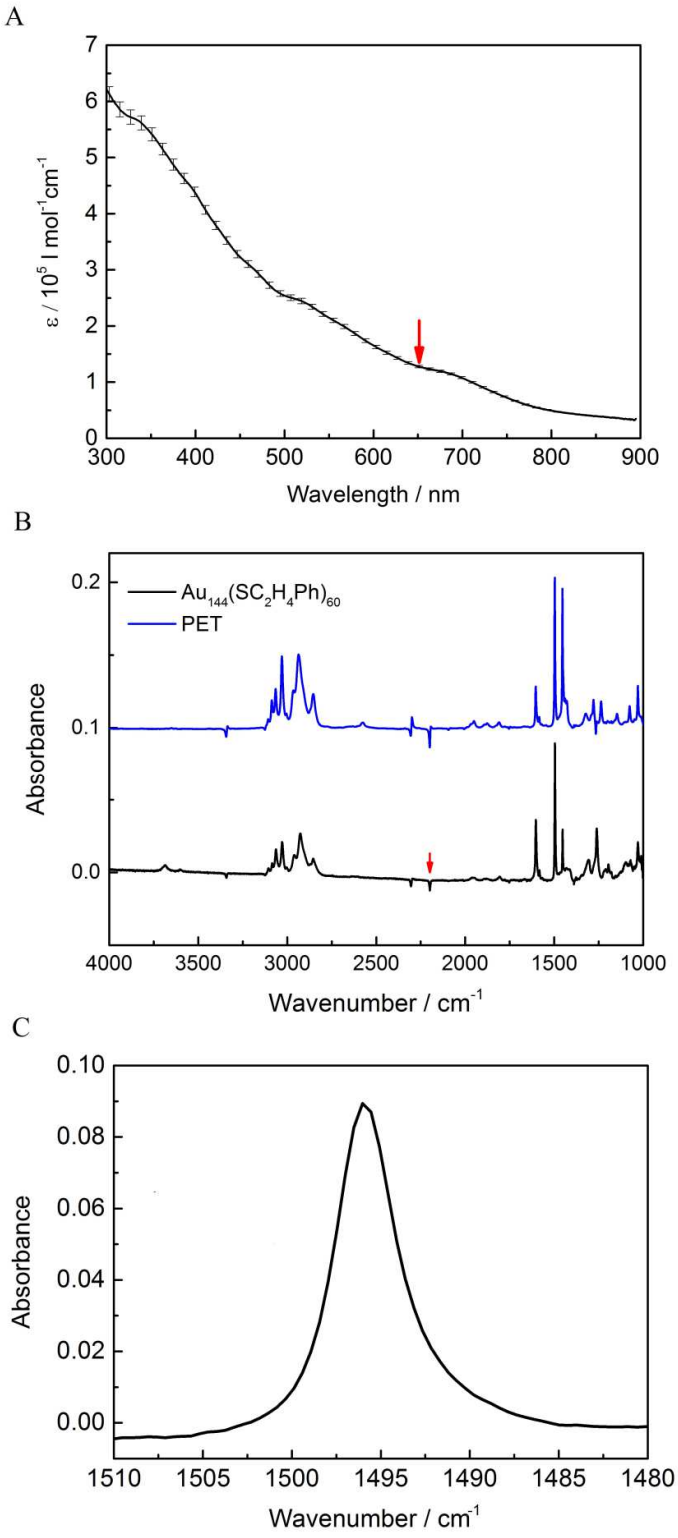


Figure 11. A) UV/Vis spectrum of $Au_{144}(SC_2H_4Ph)_{60}$. B) FTIR spectrum $Au_{144}(SC_2H_4Ph)_{60}$ and PET ligand in DCM-D2. C) Enlarged view of the vibrational mode used for probing.

For the transient absorption experiment a suitable visible pump and mid-IR probe wavelengths can be determined from the steady-state spectra. The pump wavelength was chosen to be 652 nm, which is marked with a red arrow in Fig. 11A. DFT calculations were used to confirm that the excitation is highly localized in the gold core. The probe wavelength was chosen based on the vibrational spectrum. In order to be able to study the electronic relaxation, the probed vibrational mode was selected from the region of the spectrum where there is no electronic absorption. Based on its strong absorbance, the vibrational mode at ~1495 $cm^{-1}$ was chosen. An enlarged view of the FTIR spectrum of the mode is shown in Fig. 11C. The vibrational mode was identified based on calculations and comparison to identified vibrational modes for monosubstituted benzenes as one of the vibrational modes of the benzene ring of the ligand molecules.[77]

The mid-IR transient absorption spectrum of $Au_{144}(SC_2H_4Ph)_{60}$ is shown in Fig. 12A. The spectrum shows a strong broad positive feature in the short time delays together with a negative bleach signal and a positive hot band signal of the probed mode. The kinetics for different features is shown in Fig. 12B. By using global fitting, two time constants were obtained for the relaxation processes. The faster time constant describing the initial positive feature was found to be 1.5 ps, while the longer time constant describing the behavior of the vibrational band was determined to be 29 ps.

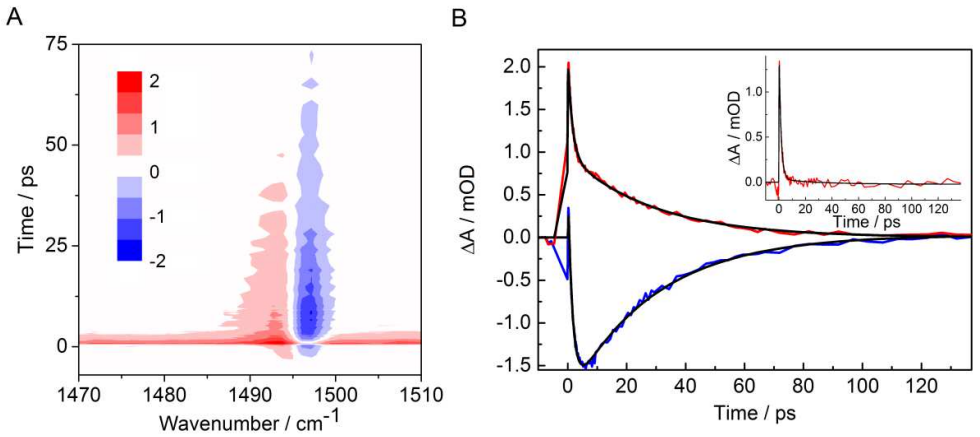


Figure 12. A) A contour plot of the transient absorption spectrum of $Au_{144}(SC_2H_4Ph)_{60}$. The color scale is in mOD. B) Kinetics at the hot band (red) and bleach band (blue). The fits to kinetics are shown in black. The inset shows kinetics at 1510 $cm^{-1}$.

The broad and short-lived low energy absorption might be indicative of generation of hot electron gas after excitation, which has been previously observed for gold clusters and also for conduction band electrons in semiconductors.[22,78] The strong broad positive signal is, therefore, attributed to the excited state absorption of the electrons of the gold core. Behavior of this type of signal

can be explained by relaxation in metallic systems as described in Section 2.5.6.3. The relaxation in metallic systems first proceeds via electron–electron scattering. This process is too fast to be observed separately in the performed experiment. The following electron–phonon scattering during which the energy is transferred to vibrational energy is observed as a decreasing excited state absorption signal. The faster time constant can, therefore, be assigned to relaxation of the initially excited electrons.

According to the two-temperature model presented in Section 2.5.6.4, for metallic systems the electronic relaxation time depends on the initial electronic temperature and hence from the total excitation energy deposited to the cluster by the pump pulse. Based on the model and on the interpretation of the short lived electron signal, a linear excitation energy dependence of the relaxation time constant should be observed. To test this, a set of experiments in which the excitation pulse energy was changed was carried out. The results shown in Fig. 13 can be used to confirm the expected linear dependence.

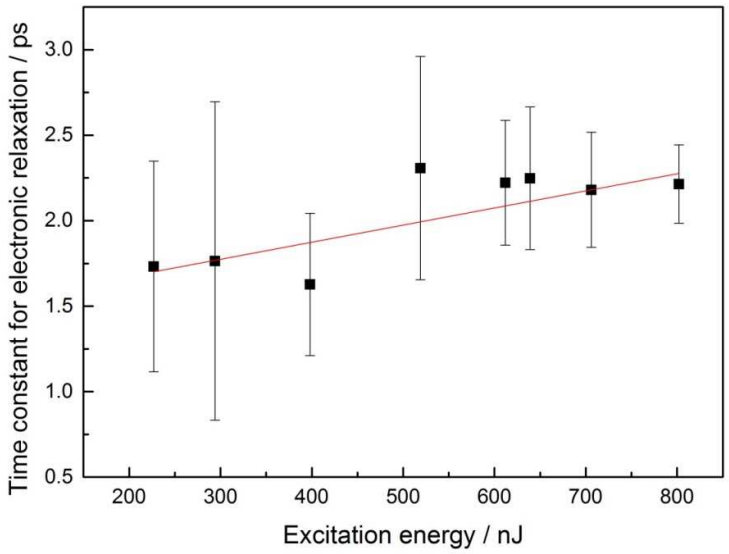


Figure 13. The excitation energy dependence of the electronic relaxation time constant for $Au_{144}(SC_2H_4Ph)_{60}$. The red line shows a linear fit to the presented data points.

The electronic relaxation is followed by the vibrational cooling of the system as the energy is transferred from the vibrations of the core to the ligands and is subsequently dissipated to the surrounding solvent system. The longer time constant (29 ps) can be attributed to the vibrational cooling of the cluster. Based on the transient absorption results, it can be shown that the energy is rapidly transferred from the excited electrons to phonons and that the absorption of the ligand vibrational mode is shifted from its ground state position. This implies that the vibrational modes of the ligands are strongly coupled to the vibrational modes of the Au–S interface and the modes of the gold core. It can

also be seen that the electronic excitation energy is rapidly and efficiently transferred into heat.

Based on the observed photodynamics and their interpretation, it can be stated that the $Au_{144}(SC_2H_4Ph)_{60}$ cluster behaves like a metallic system with no significant energy gap. The obtained photodynamics results confirm the reported results from transient absorption in the UV/vis region for $Au_{144}$ species with organosoluble and water soluble ligands.[46,47] Based on these results, the $Au_{144}$ species has been shown to be the smallest known cluster to exhibit metallic behavior. In addition to the metallic behavior, information about the vibrational relaxation is obtained.

## 4.2 $Au_{102}(p\text{MBA})_{44}$[II]

The UV/vis spectrum of $Au_{102}(p\text{MBA})_{44}$ is shown in Fig. 7. Since the electronic spectrum of this species has been previously studied in detail[40], the measured spectrum could be used to confirm the monodispersity of the sample by comparing the results. FTIR spectrum of the sample was also measured and is shown in Fig. 14. The spectrum is consistent with previously published spectra and also the spectrum of the *p*MBA ligand.[40] Due to strong solvent absorption, the spectral region from ~2000 $cm^{-1}$ to ~3000 $cm^{-1}$ could not be measured. Again, the electronic absorption of the cluster is clearly seen at the higher energy region of the spectrum.

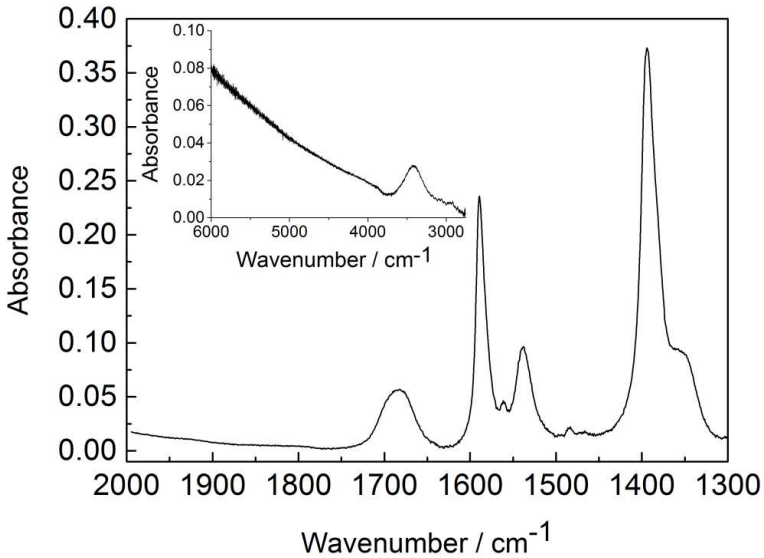


Figure 14. FTIR spectrum of $Au_{102}(p\text{MBA})_{44}$ in $D_2O$. The higher energy region is shown in the inset.

The appropriate pump and probe wavelengths could be chosen based on the measured spectra for the purpose of the photodynamics studies as done for $Au_{144}(SC_2H_4Ph)_{60}$[I]. The primary excitation wavelength was chosen to be 652 nm. The experiment was also repeated with two NIR excitation wavelengths, 1304 nm and 1518 nm, to assist the assignment of the relaxation dynamics. Again computational results were used to confirm that the excitation is mainly localized in the gold core. The absorption band at ~1400 $cm^{-1}$ was chosen as the probed vibrational mode.

A contour plot of the transient absorption spectrum is shown in Fig. 15. The transient absorption spectrum shows a negative bleach band that seems to disappear in about 20 ps, and a hot band that extends beyond the experimental window of the experiment and shows relaxation processes in different time scales.

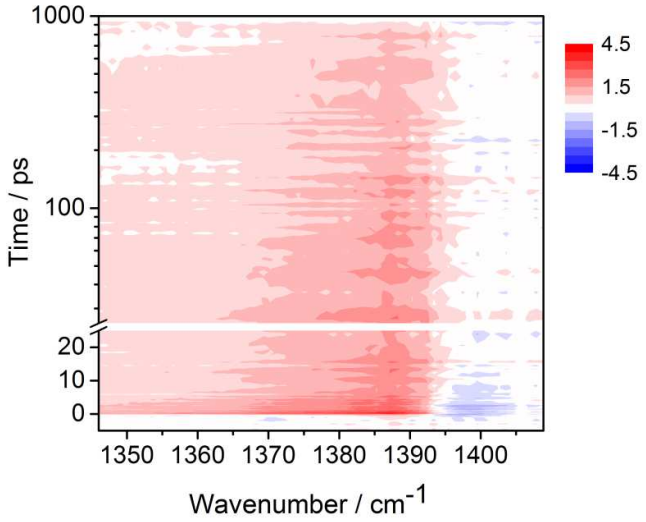


Figure 15. A contour plot of mid-IR transient absorption spectrum for $Au_{102}(p\text{MBA})_{44}$. The color scale is in mOD.

Relaxation kinetics was analyzed by separately fitting the hot band maximum, and the bleach signal. The resulting time constants were 6.8 ps for the bleach and 1.5 ps, 84 ps, and ~3.5 ns for the hot band. The fitted kinetics is shown in Fig. 16. The kinetics results of the NIR excitation experiments were analyzed similarly, and the shortest relaxation time constant was found to decrease as the excitation wavelength increases. The results are shown in Fig. 16, and the obtained time constants and the relative amplitudes of different components for the hot band kinetics are shown in Table 1. The relaxation time constants were found to be independent of the pump fluence.

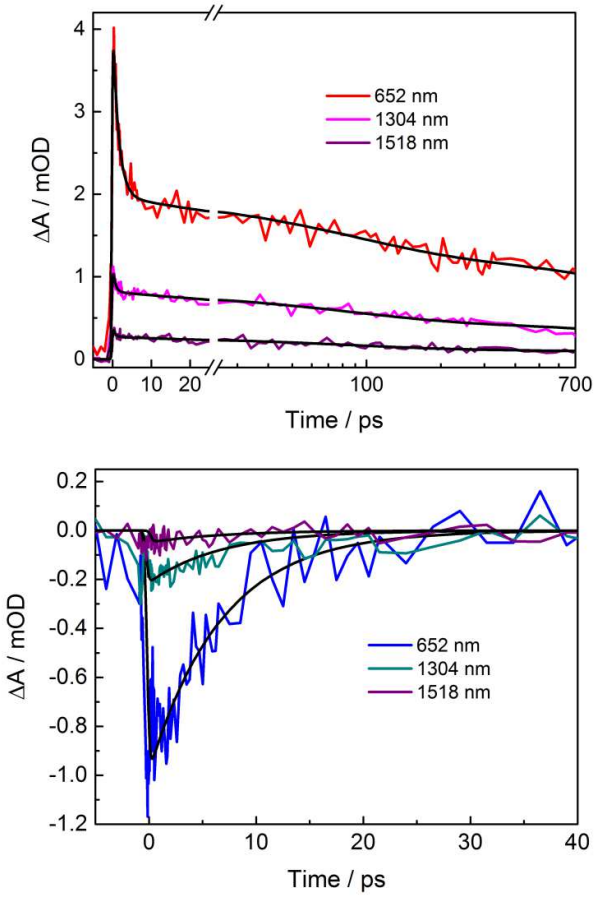


Figure 16. The kinetics obtained with different excitation wavelengths for hot band maximum (upper panel) and for bleach (lower panel). Exponential fits to data are shown in black. Reprinted with permission from paper II. Copyright 2015 American Chemical Society.

Table 1. The relaxation time constants obtained with different excitation wavelengths. The percentage of the relaxation component is also shown.

| **Excitation wavelength** | $\tau_1$ | $\tau_2$ | $\tau_3$ | $\tau_4$ |
|---|---|---|---|---|
| **652 nm** | 1.5 ps | 84 ps | ~3.5 ns | 6.8 ps |
| | 55.3 % | 16.1 % | 28.6 % | |
| **1304 nm** | 600 fs | 84 ps | ~3.5 ns | 6.8 ps |
| | 35.3 % | 28.7 % | 36.0 % | |
| **1518 nm** | 500 fs | 84 ps | ~3.5 ns | 6.8 ps |
| | 40.2 % | 33.2 % | 26.5 % | |

To more closely analyze the bleach kinetics, which appears to significantly differ from the hot band kinetics, the transient spectrum at different time delays was fitted. The fitted spectra for few a time delays are shown in Fig. 17A. Amplitude of the fitted bleach component shows long-lived kinetics hidden by the overlapping bands, which explains the seemingly asymmetric bands. The kinetics obtained for the bleach band by fitting is shown in Fig. 17B.

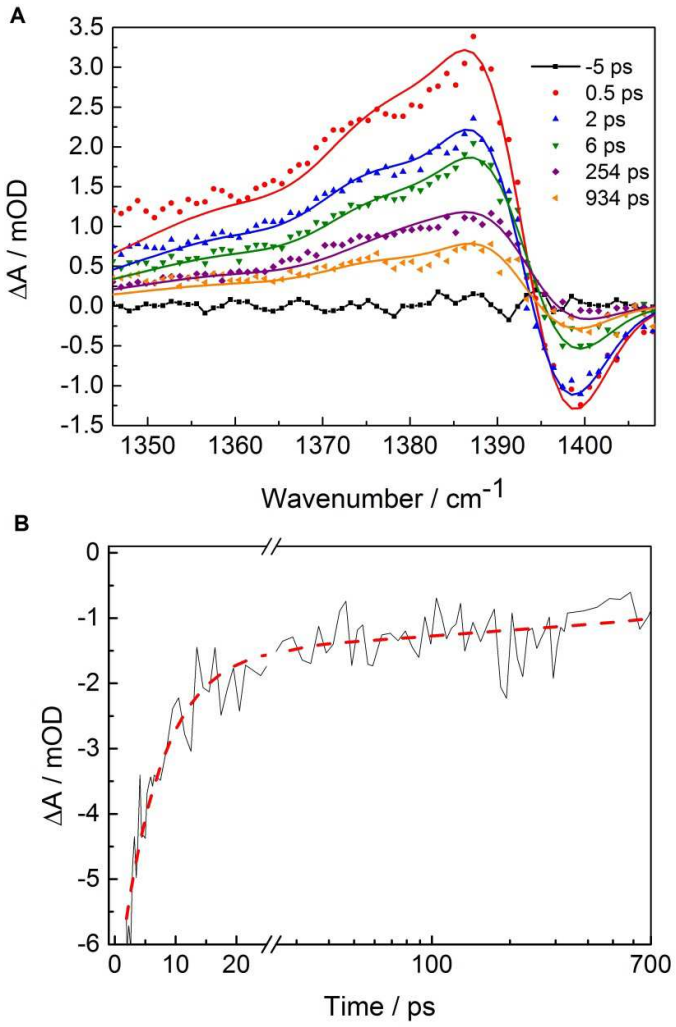


Figure 17. A) The fitted transient spectra with different time delays. B) Bleach recovery kinetics obtained by spectral fitting and extracting the time dependent amplitude of the bleach component. The red dotted line shows the bleach recovery kinetics fitted with a sum of obtained time constants 6.8 ps, 84 ps, and 3.5 ns. Reprinted with permission from paper II. Copyright 2015 American Chemical Society.

Since the observed relaxation shows long-lived excited species and the relaxation time constants are observed to be independent of the pump fluence,

the relaxation of the cluster is consistent with molecular behavior and the existence of a HOMO–LUMO gap. The observed kinetics also matches nicely with reported UV/vis transient absorption results.[47] Since the relaxation dynamics confirms the molecular behavior of the cluster, the observed kinetics was explained by using processes commonly used for molecules. For this purpose, the electronic energy levels of the cluster in singlet and triplet states were calculated. Based on this, it was observed that the geometric arrangement of the core atoms slightly changes as the spin state of the cluster changes. This was taken into account by also relaxing the triplet state structure and by calculating the energy states in different spin states in both geometries. The calculated energy levels and a summary of the interpretation of the relaxation dynamics is presented in Fig. 18.

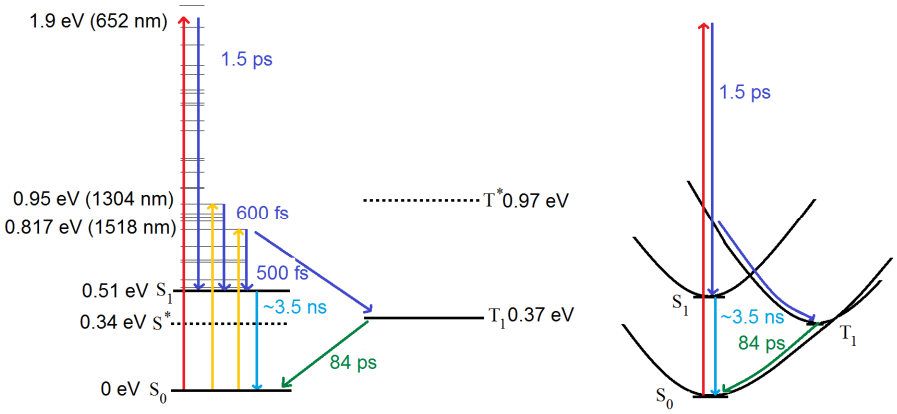


Figure 18. The computational energy levels and a summary of the interpretation of the relaxation dynamics for $Au_{102}(p\text{MBA})_{44}$ cluster. The T* and S* indicate the first excited triplet state in singlet state geometry and the ground state in triplet state geometry, respectively.

The fastest relaxation time constant (0.5–1.5 ps) was interpreted to represent the electronic relaxation from the originally excited states to the lower singlet and triplet states. The time constant cannot be assigned to a specific process but is attributed to various relaxation processes facilitated by the heating of the cluster due to simultaneous vibrational relaxation. The fast relaxation time constant is consistent with the high density of electronic states in the cluster and corresponds well with the electronic relaxation observed for $Au_{144}$ species.[I,46,47] The high density of states can also facilitate relaxation via one-phonon processes, and the initial relaxation is interpreted to involve several processes including multiple internal conversions and intersystem crossings between singlet and triplet manifolds. The intersystem crossing is presumed to occur rapidly and effectively due to the high spin–orbit coupling for the heavy gold atoms.

The excitation wavelength dependence of the shortest time constant can also be explained by this type of interpretation. It is assumed that the loss of

amplitude is associated with relaxation to the ground state, which is facilitated by excess vibrational energy that promotes sampling of curve crossings. As the amount of excess energy provided by the excitation is decreased, the potential energy surfaces of different electronic states are not sampled as efficiently; hence, the amount of time that the system spends possessing enough excess energy for curve crossings is reduced, which seemingly leads to a shorter relaxation time constant.

The longer time constants obtained from the hot band kinetics (84 ps and ~3.5 ns) can then be assigned to relaxation from the excited singlet and triplet states to the ground state. The shape of the potential energy surface of the ground state and the $S_1$ state are expected to be similar; hence, they are not expected to cross. On the other hand, based on the calculated energy levels, the energy difference between the ground state and the $T_1$ state geometry is small. Therefore, a crossing between the ground state and the $T_1$ state exists close to the $T_1$ state minimum as shown in Fig. 18. Based on this, the 84 ps time constant is assigned to relaxation from the $T_1$ state to the ground state. The remaining ~3.5 ns time constant is then assigned to the relaxation from the $S_1$ to the ground state. The $S_1$ to ground state relaxation can potentially proceed via emission, which would result in fluorescence in the mid-IR region. The situation in which the relaxation from the triplet state is faster than from the singlet state is uncommon, but based on the presented interpretation, it can be explained by the computed energy states. The remaining 6.8 ps time constant obtained from the bleach kinetics could be attributed to the vibrational cooling of the cluster.

## 4.3 $Au_{130}(p\text{MBA})_{50}^{III}$

The UV/vis and FTIR spectra of the $Au_{130}$ cluster are shown in Fig. 19, in which a comparison to the computational electronic spectrum of the $Au_{130}$ species is also shown. The computational results were obtained by utilizing DFT calculations and a model for the cluster structure proposed in Ref. 31.

Based on computational results, the HOMO–LUMO gap of the $Au_{130}(SH)_{50}$ cluster is 0.22 eV, but the stronger absorptions appear with energies higher than 0.55 eV. This result is consistent with the FTIR spectrum of the studied cluster shown in Fig. 19B. An accurate value for the onset of the electronic absorption for this cluster could not be obtained due to the solvent absorption and the absorption of OH stretching mode of the residual water in the region of interest. However, optical gap of the studied cluster can be narrowed to 2000–4300 $cm^{-1}$ region.

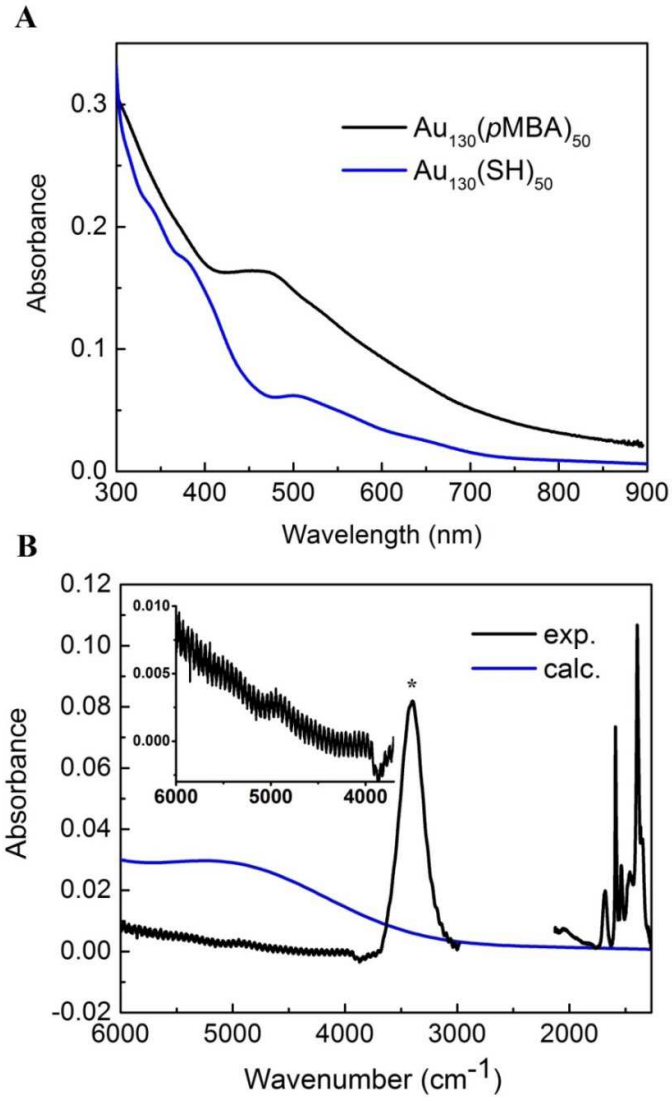


Figure 19. A) The UV/vis spectrum of the studied cluster (black), the computational spectrum for $Au_{130}(SH)_{50}$ (blue). B) FTIR spectrum of the studied cluster (black) and the computational electronic spectrum for $Au_{130}(SH)_{50}$ (blue). The absorption band marked with an asterisk (*) is induced by the OH stretching vibration of residual water. The inset shows an enlarged image of the optical absorption region of the spectrum. Reprinted with permission from paper III. Copyright 2015 American Chemical Society.

The transient absorption experiment was, again, performed by using 652 nm as excitation wavelength. The vibrational mode used for probing for $Au_{102}$ cluster was also used for $Au_{130}$ species. A contour plot of the transient spectrum of the sample is shown in Fig. 20A. The spectrum qualitatively resembles that obtained for $Au_{102}(p\text{MBA})_{44}$, since a strong, positive hot band and a bleach signal that seemingly disappears after ~20 ps are observed. The kinetics obtained for the hot band maximum and the bleach are shown in Fig. 20B.

No pump fluence dependence of the kinetics was observed when the excitation energy was changed between ~100–350 nJ.

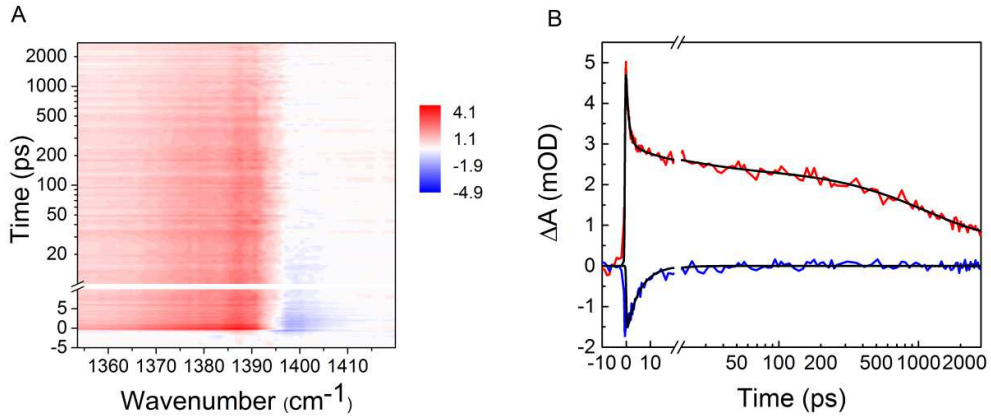


Figure 20. A) A contour plot of transient absorption spectrum for $Au_{130}$ species. The color scale is in mOD. B) The kinetics obtained for the hot band maximum and the bleach signals for $Au_{130}$ cluster. Reprinted with permission from paper III. Copyright 2015 American Chemical Society.

Five different relaxation processes could be resolved for the cluster by fitting the kinetics for the bleach and the hot band. The obtained time constants were 5.6 ps for the bleach kinetics and 1.2 ps, 20 ps, and 1.2 ns for the hot band kinetics. In addition, a long-lived constant component was observed in the hot band kinetics. Relaxation time constant for this process was estimated to be >10 ns.

The long-lived excited species and the pump energy independence of the kinetics clearly indicate molecular behavior and the existence of a significant energy gap. To explain the observed relaxation dynamics, a procedure similar to that used for $Au_{102}$ species was utilized. The interpretation of the occurring relaxation processes was again strongly based on electronic energy states calculated for the singlet and triplet states of the $Au_{130}(SH)_{50}$ cluster, which was chosen as a model based on the cluster assignment. A small change in the geometry of the core atoms is associated with the change in the spin state also for the $Au_{130}$ cluster. Therefore, the triplet state geometry is relaxed separately and the energy states are calculated also in this geometry. The computational energy levels and a summary of the interpretation of the relaxation dynamics is presented in Fig. 21.

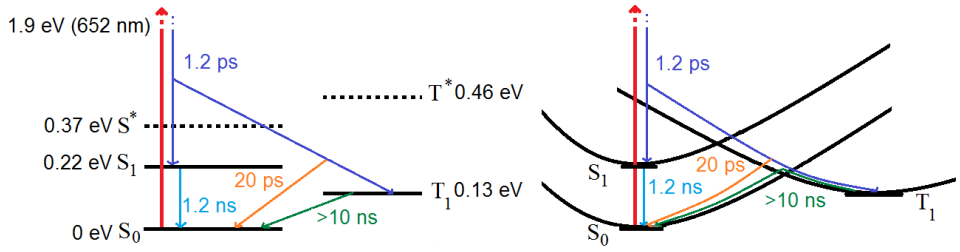


Figure 21. The summary of energy levels and interpretation of the relaxation processes for $Au_{130}(p\text{MBA})_{50}$. T* is the energy of $T_1$ state in singlet state geometry, and the S* is the ground state energy in triplet state geometry.

The shortest relaxation time constant (1.2 ps) can be explained by using interpretation similar to the one used for the corresponding time constant observed for $Au_{120}(p\text{MBA})_{44}$ cluster. Based on this, the time constant can be attributed to electronic relaxation from the initially excited state to the lowest excited singlet and triplet states. Again, the relaxation time constant cannot be assigned to a single transition but to multiple internal conversion and intersystem crossing processes leading to population in both singlet and triplet manifolds. The time constant compares well with the 1.5 ps time constant observed for the $Au_{102}(p\text{MBA})_{44}$ cluster.[II] The second shortest time constant (5.6 ps) obtained for the bleach band was assigned to vibrational relaxation.

Based on the calculated energy levels in singlet and triplet manifolds, the longer time constants could be assigned to relaxation processes occurring from the $S_1$ and $T_1$ states. For the relaxation from the $S_1$ state to the ground state, the process was estimated to occur faster than for $Au_{102}$ because of the reduced size of the gap. Therefore, the 1.2 ns time constant was assigned to this process. The remaining time constants were then related to the relaxation from the triplet state to the ground state. Based on the calculations, the ground state energy level in the triplet state geometry is 0.24 eV higher than in the triplet state geometry. Therefore, an energy barrier is presumed to exist between the triplet state and the ground state, which significantly slows down the relaxation due to the required activation energy. The long-lived excited state with a relaxation time constant >10 ns is, therefore, assigned to the relaxation from the triplet state. The 20 ps time constant is assigned to the relaxation from the triplet state during the vibrational relaxation. During the vibrational cooling of the system, there is excess vibrational energy, which facilitates the crossing of the barrier and hence a rapid intersystem crossing from the triplet state to the ground state. After the vibrational cooling, the population is trapped in the triplet state and relaxes more slowly through a thermally activated process.

The presented interpretation of the results implies that there is a long-lived excited triplet state involved in the relaxation processes. This would imply that the cluster can become transiently magnetic. In addition, it is possible that there is a small population in the triplet state, since the energy difference between the ground state and the first excited triplet state is small. This idea was

tested by measuring the EPR spectrum of the sample. However, no signal that could be assigned to the cluster was observed.

## 4.4 Changing from molecular to metallic behavior

By combining the size-dependent information obtained for the studied clusters,[I–III] the fundamental question of the molecular or metallic nature of the systems can be addressed. As stated in Section 2.3.6, this question for the thiol-protected clusters has been of high interest during the past few years[19,27,46,47] and the work presented in this thesis makes a significant contribution to this discussion.

The $Au_{144}$ species has been identified as the smallest known metallic cluster.[I,46,47] On the other hand, $Au_{102}$ has clearly been identified as a molecular species.[47,II] The results of two different research groups agree well on these cluster sizes. The drastic difference between the behaviors of the two cluster sizes differing only by 42 gold atoms in size is fundamentally important and can be used to significantly narrow the transition region between molecular and metallic behavior.

The size region between 102 and 144 gold atoms has been addressed in simultaneous work by different research groups.[III,27,47] Based on the work presented in this thesis, the region can be further narrowed to be between 130 and 144 gold atoms.[III] Based on the results of other research groups, it has been concluded that $Au_{133}$ cluster and clusters with approximate size of 115 and 117 gold atoms are non-metallic.[27,47] However, the relaxation dynamics of these clusters show no long-lived relaxation components. To narrow the transition region even further more studies are needed.

## 4.5 Implications of the results for future work

The results presented in this thesis show that the mid-IR transient absorption is a good method for the determination of the photodynamics of the thiol protected clusters and can be used to provide evidence about the existence or non-existence of the energy gap. Compared to the UV/vis transient absorption the method provides additional information about the vibrational relaxation and its role in the relaxation process. In addition, some of the spectral features of the clusters overlap severely in the UV/Vis region, making it difficult to analyze the results. In these cases, a study in the mid-IR region might provide additional information about the relaxation processes.

The presented interpretation of the relaxation dynamics for the $Au_{102}(p\text{MBA})_{44}$ cluster implies that the relaxation of the long-lived population in the excited singlet state can relax via emitting a photon. Since the HOMO–LUMO gap corresponds to emission in the mid-IR region, it would be interesting to study this further since fluorescence is rarely observed in this energy re-

gion. In addition, the implied magnetic properties of the $Au_{130}$ species could be potentially utilized in applications. In addition, further evidence about the magnetic properties would be important for verifying the interpretation shown in paper III.

# 5 SUMMARY AND CONCLUSION

Three thiol-protected gold nanoclusters, $Au_{144}(SC_2H_4Ph)_{60}$, $Au_{102}(p\text{MBA})_{44}$ and $Au_{130}(p\text{MBA})_{50}$, were characterized by optical and electronic spectroscopy and their photodynamics was studied by transient absorption in the mid-IR region with visible excitation. The observed relaxation dynamics for each cluster was analyzed, and the relaxation processes involved were identified. The results were also used to determine the molecular or metallic behavior of the cluster.

Based on the drastic difference between relaxation dynamics of $Au_{102}(p\text{MBA})_{44}$ and $Au_{130}(p\text{MBA})_{50}$ when compared to the $Au_{144}(SC_2H_4Ph)_{60}$ cluster, it could be clearly seen that the $Au_{102}$ and $Au_{130}$ species show molecular behavior while the $Au_{144}$ cluster is metallic. The results presented in this thesis can, therefore, be used to narrow the size region in which the transition from molecular to metallic occurs to be between 130 and 144 gold atoms. This information is of fundamental importance when considering not only the clusters, but also gold as a metal.

The relaxation dynamics of the $Au_{144}$ species could be explained by processes typically occurring in metallic systems. The photodynamics observed for the molecular clusters, on the other hand, could be explained by the specific electronic energy level structure of the clusters. For both clusters, the relaxation was shown to include multiple relaxation processes involving both the singlet and triplet states. Based on the relative energies of the singlet and triplet states in different spin state cluster geometries, the observed differences in relaxation kinetics could also be explained. For the $Au_{102}$ species, a fast (84 ps) relaxation via a triplet state was observed due to energy surface crossing, while a slow relaxation (>10 ns) due to an energy barrier and a thermally activated process were observed for $Au_{130}$. For both clusters, the role of vibrational cooling was also found to be significant, since the excess energy controlled by the vibrational cooling facilitates many of the observed relaxation processes.

The interpretations of the observed relaxation also have interesting implications for potential future work. The potential fluorescence in the mid-IR region from the $Au_{102}$ cluster, and the transient magnetic properties implied for

the $Au_{130}$ species may provide interesting possibilities for fundamental research and also for applications.

## REFERENCES


1. Louis, C.; Pluchery, O. *Gold Nanoparticles for Physics, Chemistry and Biology*, Imperial College Press, UK, 2012.
2. Johnston, R. L. *Atomic and Molecular Clusters*, Taylor & Francis, UK, 2002.
3. Atkins, P.; de Paula, J., *Physical Chemistry*, 8th edition, Oxford University Press, UK 2006.
4. Hollas, J. M., Modern Spectroscopy, 4th edition, John Wiley & Sons, Ltd., UK, **2008**.
5. Turro, N. J., *Modern Molecular Photochemistry*, University Science Books, USA, 1991.
6. Zewail, A. H., *J. Phys. Chem. A*, **2000**, *104*, 5660–5694.
7. Schmidbaur, H.; Cronje, S.; Djordjevic, B.; Schuster, O., *Chem. Phys.*, **2005**, *311*, 151–161.
8. Housecroft, C.E.; Sharpe, A.G., *Inorganic Chemistry*, 2nd edition, Pearson Education Limited, UK, **2005**.
9. Kreibig, U.; Vollmer, M., *Optical Properties of Metal Clusters*, Springer, Germany, 1995.
10. Tsukuda, T., *Bull. Chem. Soc. Jpn.*, **2012**, *85*, 151–168.
11. Jain, P. K.; Huang, X.; El-Sayed, I. H.; El-Sayed, M. A., *Acc. Chem. Res.*, **2008**, *41*, 1578–1586.
12. Hutter, E.; Fendler, J. H., *Adv. Mater.*, **2004**, *16*, 1685–1706.
13. Qian, H.; Zhu, M.; Wu, Z.; Jin, R., *Acc. Chem. Res.*, **2012**, *45*, 1470–1479.
14. Häkkinen, H. *Nat. Chem.* **2012**, *4*, 443−455.
15. Ulman, A., *Chem. Rev.* **1996**, *96*, 1533–1554.
16. Brust, M., Walker, M.; Bethell, D.; Schiffrin, D. J.; Whyman, R., *J. Chem. Soc., Chem. Commun.*, **1994**, 801–802.
17. Qian, H.; Jin, R., *Chem. Mater.* **2011**, *23*, 2209–2217.
18. Levi-Kalisman, Y.; Jadzinsky, P.D.; Kalisman, N.; Tsunoyama, H.; Tsukuda, T.; Bushnell, D. A.; Kornberg, R. D., *J. Am. Chem. Soc.*, **2011**, *133*, 2976–2982.
19. Negishi, Y.; Nakazaki, T.; Malola, S.; Takano, S.; Niihori, Y.; Kurashige, W.; Yamazoe, S.; Tsukuda, T.;Häkkinen, H. *J. Am. Chem. Soc.* **2015**, *137*, 1206–1212.
20. Negishi, Y.; Nobusada, K.; Tsukuda, T., *J. Am. Chem. Soc.*, **2005**, *127*, 5261–5270.
21. Hassan, S.; Schade, M.; Shaw, C. P.; Lévy, R.; Hamm, P., *J. Phys. Chem. B*, **2014**, *118*, 7954–7962.
22. Schade, M.; Moretto, A.; Donaldson, P. M.; Toniolo, C.; Hamm, P. *Nano Lett.* **2010**, *10*, 3057−3061.
23. Jupally, V. R.; Dass, A., *Phys. Chem. Chem. Phys.*, **2014**, *16*, 10473–10479.
24. Chen, Y., Zeng, C., Kauffman, D. R.; Jin, R., *Nano Lett.*, **2015**, *15*, 3603–3609.

25. Jadzinsky, P. D.; Calero, G.; Ackerson, C. J.; Bushnell, D. A.; Kornberg, R. D. *Science* **2007**, *19*, 430−433.
26. Chen, Y.; Zeng, C.; Liu, C.; Kirschbaum, K.; Gayathri, C.; Gil, R. R.; Rosi, N.L.; Jin, R., *J. Am. Chem. Soc.*, **2015**, *137*,10076–10079.
27. Zeng, C.; Chen, Y.; Kirschbaum, K.; Appavoo, K.; Sfeir, M. Y.; Jin, R. *Sci. Adv.* **2015**, *1*, e1500045.
28. Zhu, M.; Aikens, C. M.; Hollander, F. J.; Schatz, G. C.; Jin, R., *J. Am. Chem. Soc.***, 2008**, *130*, 5883−5885.
29. Qian, H.; Eckenhoff, W. T.; Zhu, Y.; Pintauer, T.; Jin, R., *J. Am. Chem. Soc.*, **2010**, *132*, 8280–8281.
30. Azubel, M.; Koivisto, J.; Malola, S.; Bushnell, D.; Hura, G. L.; Koh, A. L.; Tsunoyama, H.; Tsukuda, T; Pettersson, M.; Häkkinen, H.; Kornberg, R. D., *Science*, **2014**, *345*, 909–912.
31. Negishi, Y.; Sakamoto, C., Ohyama, T.; Tsukuda, T. *J. Phys. Chem. Lett*. **2012**, *3*, 1624–1628.
32. Häkkinen, H.; Walter, M.; Grönbeck, H., *J. Phys. Chem. B*, **2006**, *110*, 9927–9931.
33. Balletto, F.; Ferrando, R., *Rev. Mod. Phys.*, **2005**, *77*, 371–423.
34. Knoppe, S.; Dolamic, I; Dass, A.; Bürgi, T., *Angew. Chem. Int. Ed.*, **2012**, *51*, 7589–7591.
35. Walter, M., Akola, J., Lopez-Acevedo, O., Jadzinsky, P., Calero, G., Ackerson, C.V., Whetten, R. L., Grönbeck, H., Häkkinen, H. *PNAS*, **2008**, *105*, 9157–9162.
36. Hartland, G.V., *Chem. Rev.* **2011**, *111*, 3858–3887.
37. Koskinen, M.; Lipas, P.O.; Manninen, M., *Z. Phys. D*, **1995**, *35*, 285–297.
38. Martin, T. P.; Bergmann, T.; Göhlich, H.; Lange, T. *J. Phys. Chem.* **1991**, *95*, 6421–6429.
39. Aikens, C. M., *J. Phys. Chem. C*, **2008**, *112*, 19797–19800.
40. Hulkko, E., Lopez-Acevedo, O., Koivisto, J., Levi-Kalisman, Y., Kornberg, R.D., Pettersson M., Häkkinen, H. *J. Am. Chem. Soc.* **2011**, *133*, 3752–3755.
41. Philip, P.; Chantharasupawong, P.; Qian, H.; Jin, R.; Thomas, J. *Nano Lett.* **2012**, *12*, 4661–4667.
42. Malola, S.; Lehtovaara, L.; Enkovaara, J.; Häkkinen, H. *ACS Nano*, **2013**, *7*, 10263–10270.
43. Smith, B.A.; Zhang, J. Z.; Giebel, U.; Schmid, G. *Chem. Phys. Lett.*, **1997**, *270*, 139–144.
44. Taylor, K., J.; Pettiette-Hall, C. L.; Cheshnovsky, O.;Smalley, R.E., *J. Chem. Phys.*, **1992**, *96*, 3319–3329.
45. Lin, X.; Nilius, N.; Freund, H.-J.; Walter, M.; Frondelius, P.; Honkala, K.; Häkkinen, H., *Phys. Rev. Lett.*, **2009**, *102*, 206801.
46. Yi, C.; Tofanelli, M. A.; Ackerson, C. J.; Knappenberger, K. L., Jr., *J. Am. Chem. Soc.* **2013**, *135*, 18222–18228.
47. Yi, C.; Zheng, H.; Tvedte, L. M.; Ackerson, C. J.; Knappenberger, K. L., Jr., *J. Phys. Chem. C*, **2015**, *119*, 6307–6313.

48. Green, T. D.; Knappenberger, K. L., Jr., *Nanoscale*, **2012**, *4*, 4111–4118.
49. Miller, S. A.; Womick, J. M.; Parker, J. F.; Murray, R. W.; Moran A. M., *J. Phys. Chem. C* **2009**, *113*, 9440–9444.
50. Sfeir, M., Y.; Qian, H.; Nobusada, K.; Jin, R., *J. Phys. Chem. C*, **2011**, *115*, 6200–6207.
51. Qian, H.; Sfeir, M. Y.; Jin, R., *J. Phys. Chem. C*, **2010**, *114*, 19935–19940.
52. Link, S.; El-Sayed, M. A.; Schaaf, T. G.; Whetten, R.L., *Chem. Phys. Lett.*, **2002**, *356*, 240–246.
53. Grant, C. D.; Schwartzberg, A. M.; Yang, Y.; Chen, S.; Zhang, J.Z., *Chem. Phys. Lett.*, **2004**, *383*, 31–34.
54. Varnavski, O.; Ramakrishna, G.; Kim, J.; Lee, D.; Goodson, T., *J. Am. Chem. Soc*. **2010**, *132*, 16−17.
55. Salorinne, K.; Lahtinen, T.; Malola, S.; Koivisto, J.; Häkkinen, H. *Nanoscale* **2014**, *6*, 7823–7826.
56. Koivisto, J., Salorinne, K., Mustalahti, S., Lahtinen, T., Malola, S., Häkkinen, H., Pettersson, M. *J. Phys. Chem. Lett.* **2014**, *5*, 387–392.
57. Wong, O. A.; Heinecke, C. L.; Simone, A. R.; Whetten, R. L.; Ackerson, C. J. *Nanoscale*, **2012**, *4*, 4099–4102.
58. Varnholt, B; Oulevey, P.; Luber, S.; Kumara, C.; Dass, A.; Bürgi, T., *J. Phys. Chem. C*, **2014**, *118*, 9604–9611.
59. Heinecke, C. L.; Ni, T. W.; Malola, S.; Mäkinen, V.; Wong, O. A.; Häkkinen, H.; Ackerson, C. J., *J. Am. Chem. Soc.*, **2012**, *134*, 13316–13322.
60. Marjomäki, V.; Lahtinen, T.; Martikainen, M.; Koivisto, J.; Malola, S.; Salorinne, K.; Pettersson, M.; Häkkinen, H., *PNAS*, **2014**, *111*, 1277–1281.
61. Lopez-Acevedo, O.; Akola, J.; Whetten, R. L.; Grönbeck, H.; Häkkinen, H. *J. Phys. Chem. C* **2009**, *113*, 5035−5038.
62. Hicks, J.F.; Miles, D.T., Murray, R.W., *J. Am. Chem. Soc.*, **2002**, *124*, 13322–13328.
63. Koivisto, J.; Malola, S.; Kumara, C.; Dass, A.; Häkkinen, H.; Pettersson, M. *J. Phys. Chem. Lett.* **2012**, *3*, 3076−3080.
64. Tang, Z.; Robinson, D. A.; Bokossa, N.; Xu, B.; Wang, S.; Wang, G. *J. Am. Chem. Soc.* **2011,** *133*, 16037–16044.
65. Tlahuice-Flores, A.; Santiago, U.; Bahena, D.; Vinogradova, E.; Conroy, C.V.; Ahuja, T.; Bach, S. B. H; Ponce, A.; Wang, G.; José-Yacamán, M.; Whetten, R. L., *J. Phys. Chem. A*, **2013**, *117*, 10470–10476.
66. Jupally, V.R.; Thrasher, J. G., Dass, A., *Analyst*, **2014**, *139*, 1826–1829.
67. Dolamic, I.; Varnholt, B.; Bürgi, T., *Phys. Chem. Chem. Phys.*, **2013**, *15*, 19561–19565.
68. Rulliere, C., *Femtosecond Laser Pulses Principles and Experiments*, 2nd edition, Springer, USA, 2005.
69. Diels, J.-C., *Ultrashort laserpulse phenomena: fundamentals, techniques, and applications on a femtosecond time scale*, 2nd edition, Elsevier, 2006.

70. Kaganov, M. I.; Lifshitz, I. M.; Tanatarov, L. V. *Zh. Eksp. Teor. Fiz.* **1957**, *31*, 232.
71. Arbouet, A.; Voisin, C.; Cristofilos, D.; Langot, P.; Del Fatti, N.; Vallée, F.; Lermé, J.; Celep, G.; Cottancin, E.; Gaudry, M.; Pellarin, M.; Broyer, M.; Maillard, M.; Pileni, M. P.; Treguer, M., *Phys. Rev. Lett.*, **2003**, *90*, 177401.
72. Hamm, P., *Chemical Physics*, **1995**, *200*, 415–429.
73. Salorinne, K.; Lahtinen, T.; Koivisto, J.; Kalenius, E.; Nissinen, M.; Pettersson, M.; Häkkinen, H., *Anal. Chem.*, **2013**, *85*, 3489–3492.
74. Bredenbeck, J.; Hamm P. *Rev. Sci. Instrum*, **2003**, *74*, 3188–3189.
75. Hamm, P.; Kaindl, R. A.; Stenger, J., *Opt. Lett.*, **2000**, *25*, 1798–1800.
76. Macoas, E. M. S.; Kananavicius, R.; Myllyperkiö, P.; Pettersson, M.; Kunttu, H., *J. Phys. Chem. A*, **2007**, *111*, 2054–2061.
77. Gardner, A. M.; Wright, T. G. *J. Chem. Phys.* **2011**, *135*, 114305.
78. Ghosh, H. N.; Asbury, J. B.; Lian, T. *J. Phys. Chem. B* **1998**, *102*, 6482–6486.